https://doi.org/10.5194/egusphere-2025-6095
Preprint. Discussion started: 19 January 2026

Mechanisms of air-sea CO_2 exchange in the central Baltic Sea

Yuanxu Dong[1,2], Christa A. Marandino[1], Ryo Dobashi[3], David Ho[3], Gregor Rehder[4], Henry C. Bittig[4], Josefine Karnatz[1], Bita Sabbaghzadeh[4], Helen Czerski[5], Anja Engel[1]

[1]Marine Biogeochemistry Research Division, GEOMAR Helmholtz Centre for Ocean Research Kiel, Kiel, Germany

[2]Institute of Environmental Physics, Heidelberg University, Heidelberg, Germany

[3]Department of Oceanography, University of Hawai'i at Mānoa, Honolulu, Hawaii, USA

[4]Leibniz Institute for Baltic Sea Research Warnemünde, Rostock, Germany

[5]Department of Mechanical Engineering, University College London, London, UK

Correspondence to: Yuanxu Dong (ydong@geomar.de)

Abstract Air-sea gas exchange regulates the cycling of climate-relevant gases such as carbon dioxide (CO_2), yet large uncertainties remain in its quantification. The gas transfer velocity (K), a key parameter for estimating CO_2 flux, is usually expressed as a function of wind speed (U_{10N}). This approach overlooks the role of fetch and surfactants, which can substantially affect K. However, no field study has systematically quantified their combined effects under fetch-limited and surfactant-abundant ocean conditions. To fill this research gap, we conducted air-sea gas exchange studies during a cruise in the central Baltic Sea, a system with high surfactant levels and a short fetch. We report independent determinations of K using eddy covariance (EC) and dual-tracer techniques, together with direct measurements of natural surfactants and modelled wave parameters. Both methods yield consistent results; however, EC-based CO_2 transfer velocities are on average 33% lower than those reported in the open ocean in previous EC studies. Sea-state-dependent parameterisations indicate that limited fetch reduces K by 8%, while elevated surfactant concentrations may have contributed to the additional 25% reduction. We developed an updated parameterization that includes wind stress, sea state, and surfactants. When applied to climatological forcing, it yields a 40% stronger seasonal cycle of CO_2 flux in the Baltic Sea than obtained with the conventional U_{10N}-based parameterization. These findings highlight the need to move beyond U_{10N} in the parameterization of K and estimation of regional fluxes, especially when evaluating the potential of marine carbon dioxide removal (mCDR) in coastal seas.

https://doi.org/10.5194/egusphere-2025-6095
Preprint. Discussion started: 19 January 2026

Short summary Air-sea gas exchange regulates the Earth's climate. However, the description of the kinetic exchange process only uses wind speed, neglecting other drivers. In this study, we investigate how fetch and natural surfactants modulate the air-sea carbon dioxide exchange. Measurements from the central Baltic Sea show that limited fetch and elevated surfactants significantly suppress this exchange. A new parameterization is provided, improving regional carbon budgets and evaluations of climate solutions.

1. Introduction

The ocean is a major sink of carbon dioxide (CO_2) emitted by human activities, substantially mitigating climate change (Friedlingstein et al., 2025). In the context of increasing climate change, the ocean is considered a tool for solutions in addition to its natural role, through marine-based carbon dioxide removal (mCDR) (Doney et al., 2024). The accurate quantification of global ocean carbon flux and the regional mCDR efficiency is essential for climate predictions. Air-sea CO_2 flux is often estimated using the bulk formula:

$$F = K_{660}\left(\frac{Sc}{660}\right)^{-n}(\alpha_w fCO_{2w} - \alpha_i fCO_{2a}) \quad (1)$$

where F (e.g., mmol m^{-2} day^{-1}) is the air-sea CO_2 flux, K_{660} (cm h^{-1}) is the gas transfer velocity normalized to a Schmidt number (Sc) of 660, corresponding to CO_2 in seawater at 20°C. The value of the exponent n is between 1/2 and 2/3 (Jähne et al., 1987), and is often assumed to be 1/2 in the ocean environment (Wanninkhof et al., 2009). CO_2 solubilities (e.g., mol L^{-1} atm^{-1}) at the base of the mass boundary layer and at the air-sea interface are α_w and α_i, respectively. CO_2 fugacity (fCO_2, µatm) at these locations are fCO_{2w} and fCO_{2a}. Sc and α depend on water temperature and salinity (Wanninkhof, 2014; Weiss, 1974). Notably, if both the CO_2 flux and fCO_2 are known, K_{660} can be derived.

Equation 1 highlights the central role of K_{660} as the kinetic forcing parameter in air-sea CO_2 exchange. K_{660} is directly driven by near-surface turbulence, and affected by many factors near-surface processes (Garbe et al., 2014). On a global scale, wind forcing has a dominant effect on gas transfer velocity, and other factors, such as friction velocity, waves, and bubbles, are strongly linked with wind speed (Wanninkhof et al., 2009). Thus, the readily available 10-meter neutral

https://doi.org/10.5194/egusphere-2025-6095
Preprint. Discussion started: 19 January 2026

height wind speed (U_{10N}) is often used as a sole variable for the parameterization of K_{660} (e.g., Ho et al., 2006; Nightingale et al., 2000; Wanninkhof, 2014). However, wind is not the only factor driving gas exchange, as other factors that are not fully linked with the wind speed can substantially influence this exchange at regional scales, particularly in the coastal ocean (Upstill-Goddard, 2006). Existing U_{10N}-based K_{660} formulations in the Baltic Sea yield controversial results (e.g., Gutiérrez-Loza et al., 2022; Kuss et al., 2004), highlighting the lack of mechanistic understanding of air-sea gas exchange.

Surfactants are surface-active compounds, molecules, or biomolecules. They are ubiquitous in the ocean and often highly concentrated in coastal waters through biological production and terrestrial inputs (Mustaffa et al., 2020; Sabbaghzadeh et al., 2017; Wurl et al., 2011), suppressing gas exchange by damping surface turbulence and forming an additional diffusion barrier (McKenna and McGillis, 2004; Pereira et al., 2016). In contrast, wave breaking enhances gas transfer, especially for low-soluble gases, by introducing bubbles as an exchange pathway in addition to the interfacial exchange route (Bell et al., 2017; Blomquist et al., 2017; Dong et al., 2025; Woolf, 1997). Wave breaking is strongly impacted by the fetch, the distance over which wind acts on the water surface, as limited fetch suppresses wave breaking and bubble generation (Fairall et al., 2006; Kunz and Jähne, 2018; Ocampo-Torres and Donelan, 1995; Prytherch and Yelland, 2021; Woolf, 2005). Understanding how these mechanisms influence air-sea gas exchange is essential for regional (coastal) carbon budgets and for developing robust monitoring, reporting, and verification (MRV) frameworks to support mCDR strategies (e.g., Ho et al., 2023).

The Baltic Sea, with its high primary productivity (Schmidt and Schneider, 2011) in summer and limited fetch, provides an ideal natural laboratory to investigate the combined effects of surfactants and fetch on air-sea gas exchange. We therefore conducted a comprehensive gas exchange experiment in the central Baltic Sea to quantify the impact of factors additional to wind speed on gas exchange.

2. Methods

2.1 CenBASE cruise

The Central Baltic Air-Sea Exchange Experiment (CenBASE; EMB 295) was conducted in summer 2022, immediately after the phytoplankton bloom season, to capture strong air-sea gas

https://doi.org/10.5194/egusphere-2025-6095
Preprint. Discussion started: 19 January 2026

exchange signals (Parard et al., 2016; Bittig et al., 2024). The research cruise on the *R/V Elisabeth Mann Borgese* (EMB) departed from Rostock, Germany, on 2 July and returned on 18 July, with the primary study area located in the Gotland Basin (Fig. 1A).

Eddy covariance (EC) CO_2 flux observations (Section 2.2) and the dual-tracer experiment (see Appendix A1) were performed simultaneously to determine gas transfer velocities, representing the second successful joint deployment of these two approaches after GasEx-98 (Ho and Wanninkhof, 2016; McGillis et al., 2001). Surfactant samples were collected from both the microlayer and underlying water (see Appendix A2). Wave parameters were extracted from the ERA5 hourly reanalysis data product (0.5° × 0.5°) (Hersbach et al., 2020) based on the cruise track's spatiotemporal coordinates. Additional measurements included fCO_2, sea surface properties, and meteorological variables to support the analysis.

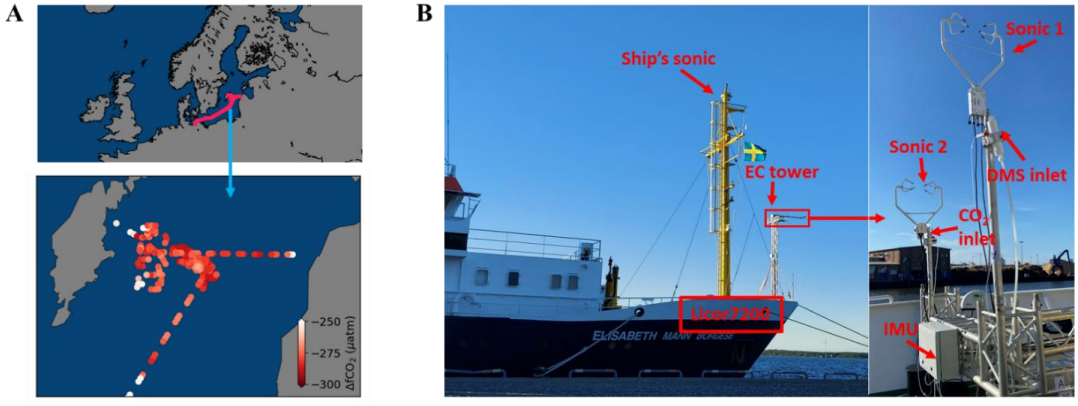

Figure 1: CenBASE cruise tracks and the ship-based eddy covariance (EC) system. Left panel: Cruise tracks in the central Baltic Sea, color-coded by air-sea CO_2 fugacity differences (ΔfCO_2). Middle panel: Research vessel EMB during the CenBASE cruise; a custom-built EC tower is mounted at the bow. Right panel: Instruments mounted on top of the tower, including sonic anemometers, a motion sensor (IMU), and the CO_2 inlet. Additional setup details are provided in Section 2.

2.2 Eddy covariance CO_2 flux measurements

The EC technique allows for direct measurements of air-sea CO_2 flux using the following equation:

https://doi.org/10.5194/egusphere-2025-6095
Preprint. Discussion started: 19 January 2026

$$F = \rho\overline{w'c'} \quad (2)$$

where ρ is the mean mole density of dry air (e.g., in mole m^{-3}), w is the vertical wind velocity (in m s^{-1}), and c is the dry air mole fraction of CO_2 (in ppm or µmol mol^{-1}). The primes denote the fluctuations from the mean, and the overbar indicates time averaging. Due to the dynamic nature of the marginal sea environment, a 10-minute averaging interval was chosen, shorter than the 20-30 minutes typically used in the open ocean (e.g., Blomquist et al., 2017). The CO_2 transfer velocity (K_{660_CO2}) is derived by combining Equations 1 and 2. The EC momentum flux is similarly calculated as $\rho\overline{w'u'}$, where u is the horizontal wind component. The friction velocity (u_*) is then derived as the square root of the momentum flux magnitude.

Most components of the EC system were mounted on a custom-built tower at the bow of the ship to minimize the flow distortion (Fig. 1B). The tower extended 5 m above the deck, reaching a height of 14 m above mean sea level (MSL). A three-dimensional (3D) sonic anemometer (CSAT3B, *Campbell Scientific*) was installed on the starboard arm to measure the wind fluctuations, with a backup unit on the port side (CSAT3). An Inertial Measurement Unit (IMU, *SBG Systems*), housed in a meteorological box at the top of the tower, recorded ship motion. The IMU was positioned 66 cm from the starboard sonic and 173 cm aft of it. CO_2 fluctuations were measured using a LI-7200 gas analyzer. The sampled air was dried with a Nafion dryer operating in 'reflux' mode (Perma Pure LLC, 2024). Air was drawn from the port-side inlet through a ~10-m Teflon tube (3/8" inner diameter) at a stable flow rate of 33.2 ± 0.3 L min^{-1}. The 20-Hz signal from the sonic anemometer, IMU, and LI-7200 were logged by a datalogger (CR6, *Campbell Scientific*).

Data processing and quality control procedures followed those described in Dong et al. (2021). Briefly, motion corrections were applied to the wind (Edson et al., 1998) and CO_2 signals (Miller et al., 2010) to remove contamination from ship motion. A nitrogen puff test revealed a 0.3 s e-fold response time, which is used to correct the high-frequency attenuation (Blomquist et al., 2014). The time delay (~2.5 s) between the inlet and the gas analyzer was assessed via the maximum covariance method. Flow distortion was minimized by mounting the EC tower arms beyond the ship's hull.

2.3 Auxiliary observations

https://doi.org/10.5194/egusphere-2025-6095
Preprint. Discussion started: 19 January 2026

The partial pressure of CO_2 in surface water was measured at 1-minute intervals using the Mobile Equilibrator Sensor System (MESS) paired with two off-axis integrated cavity output laser spectrometers (oa-ICOS, Los Gatos Instruments) (Sabbaghzadeh et al., 2021). Seawater was continuously drawn from the ship's inlet at a depth of ~3.3 m. Atmospheric CO_2 was measured daily using an air inlet mounted on the ship's foremast at 13.5 m above MSL. These air CO_2 data are compared to the absolute CO_2 values measured by the EC gas analyzer (LI-7200, LI-COR, Inc.) to generate the 10-min time series of atmospheric CO_2. Sensor calibration was performed almost daily using standard gases from the Central Analytical Laboratories of the European Integrated Carbon Observation System (ICOS RI). Mean wind measurements were obtained from a sonic anemometer mounted 17 m above MSL on the ship's foremast to minimize flow distortion (O'Sullivan et al., 2013). Residual distortion was corrected using the ERA5 reanalysis wind product and nearby station records (see Appendix A3). Atmospheric pressure and temperature at ~13.5 m MSL were recorded by the onboard weather station. Surface seawater temperature and salinity were monitored by the ship's underway system and calibrated against CTD (conductivity, temperature, and depth) casts.

In addition, wave parameters were extracted from the ERA5 analysis wave product according to the open ocean EC cruise tracks (see Yang et al., 2022) and the CenBASE cruise. The COARE model is used to estimate the bulk u_* (Edson et al., 2013). For the open ocean scenario, the environmental variables from the corresponding cruises are used as inputs for the COARE model (Yang et al., 2022). The environmental parameters observed during the CenBASE cruise are used for the Baltic Sea u_* estimate in the COARE model.

3. Results

3.1 Environmental variables and the CO_2 flux

During CenBASE, winds predominantly originated from the west to north sector (Fig. 2A), with an effective fetch of approximately 50-300 km in the main study area (Fig. A1, Appendix). The wind speed ranged from 1 to 12 m s^{-1} (Fig. 2A). Water depth across the central Baltic Sea study

https://doi.org/10.5194/egusphere-2025-6095
Preprint. Discussion started: 19 January 2026

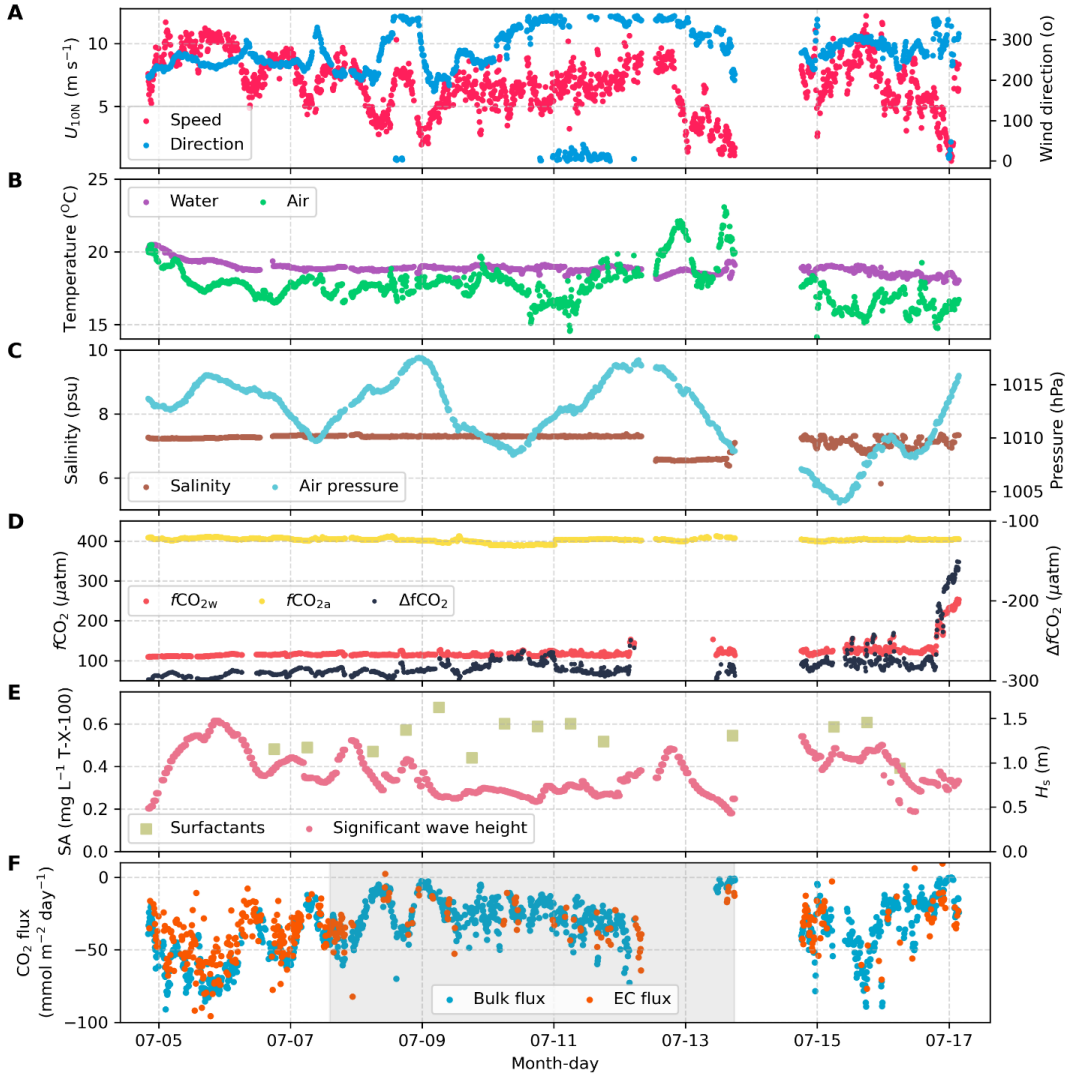

Figure 2: Ten-minute averages of environmental variables and air-sea CO_2 flux. A: Neutral 10-meter wind speed (U_{10N}, red) and wind direction (blue). **B**: Surface seawater temperature (purple) and air temperature (green). **C**: Seawater salinity (brown) and sea-level air pressure (light-blue). **D**: CO_2 fugacity in surface seawater (red) and atmosphere (yellow), and their difference (ΔfCO_2, black). **E**: Surface microlayer surfactant activity (SA, light green squares) and significant wave height extracted from ERA5 (H_s, red); **F**: Bulk CO_2 flux estimates (blue, based on K_{660} parameterisation from Ho et al., 2006) and EC CO_2 flux observations (orange). The dual-tracer tracing period is indicated by the light gray shading. Data are missing from 12-14 July due to a medical event and a temporary shortage of liquid nitrogen, which required the vessel to leave the primary study area.

https://doi.org/10.5194/egusphere-2025-6095
Preprint. Discussion started: 19 January 2026

site ranged from ~50 to 250 m. Surface water was generally warmer than the overlying air (Fig. 2B), resulting in an unstable boundary layer. Surface salinity remained consistent at approximately 7.3 throughout the study region (Fig. 2C). The cruise took place shortly after a summer phytoplankton bloom, resulting in remarkably low sea surface fCO_2 (~120 µatm; Fig. 2D). Atmospheric fCO_2 remained constant at ~403 µatm, creating a strong air-sea gradient ($\Delta fCO_2 \approx$ -280 µatm on average; Fig. 2D) that generates strong ocean CO_2 uptake signals.

Surface microlayer surfactant activity (SA), expressed as Triton-X-100 equivalents, was relatively constant at 0.54 ± 0.08 mg L^{-1} (Fig. 2E), significantly higher than typical open-ocean values (0.1-0.2 mg L^{-1}; Mustaffa et al., 2020; Sabbaghzadeh et al., 2017). Modeled significant wave height (H_s) remained below 1.5 m (Fig. 2E), lower than expected for comparable wind speeds in the open ocean (Fig. A2). Bulk CO_2 fluxes estimated from the measured ΔfCO_2 and an open-ocean dual-tracer K_{660} parameterisation (Ho et al., 2006) were higher than observed EC fluxes under high wind speeds and lower than observed EC fluxes under low wind speeds (Fig. 2F and Fig. A3). During the tracer-tracking period (8-14 July), frequent ship heading changes reduced EC flux quality, leading to most valid EC measurements from outside this period (Fig. 2F, light-gray shading). Nevertheless, as both EC and dual-tracer were collected in the same study area, the K from both methods can be reasonably considered simultaneous measurements.

3.2 Friction velocity

The friction velocity is a key parameter characterizing near-surface turbulence. Observed u_* values during CenBASE were 10% higher than in the open ocean at the same wind speeds (Fig. 3A), likely reflecting fetch-related differences. The wave field in the central Baltic Sea is much younger than the open ocean, with wave age ~60% lower at the same wind speed (Fig. 3B). The waves are shorter and steeper relative to the open ocean (Fig. A2). This wave field enhances sea surface roughness and elevates u_* relative to the open sea. u_* predicted by the COARE3.6 model, when forced with observed environmental and extracted wave parameters during CenBASE, broadly agrees with measurements (Fig. 3A). This supports that the COARE model remains largely applicable to fetch-limited marine environments when wave information is incorporated in the model, although largely developed from open-ocean observations (Edson et al., 2013). Given that u_* is an indicator of surface wind-induced turbulence, this elevated u_* is expected to enhance CO_2 transfer velocity (see Section 3.4).

https://doi.org/10.5194/egusphere-2025-6095
Preprint. Discussion started: 19 January 2026

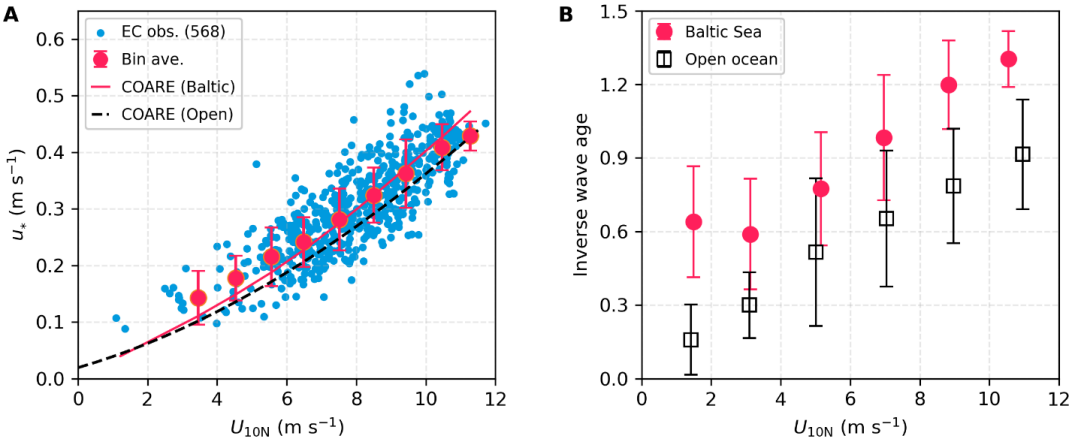

Figure 3: Friction velocity (u_*) and inverse wave age in the Baltic Sea (CenBASE) and open ocean. A: u_* derived from EC air-sea momentum fluxes versus 10-meter neutral wind speed (U_{10N}). Blue dots: 10-min u_* observations during CenBASE (568 points), with red points corresponding to bin averages (per 1 m s^{-1}). Red line: u_* simulated by COARE3.6 using the Baltic Sea environmental data; Black-dashed line: COARE3.6 simulations in the open ocean. **B:** Inverse wave age (U_{10N}/ C_p) in the Baltic Sea (red dots) and open ocean (black squares). Error bars denote ± 1 standard deviation (STD) of bin averages. The hourly wave parameters can be found in Fig. A2 in the Appendix.

3.3 Gas transfer velocities from EC and DT

The CO_2 transfer velocity (K_{660_CO2}) was derived from EC air-sea CO_2 flux and ΔfCO_2 observations using Equation 1. After quality control, 301 valid 10-min K_{660_CO2} data points were retained (Fig. 4). The large $|\Delta fCO_2|$ (~280 µatm) ensured accurate K_{660_CO2} derivations, with hourly uncertainties of ~20% (Fig. A4), substantially lower than typical cruise-based uncertainties (e.g., ~30% during the HiWinGS cruise; Blomquist et al., 2017). The cool skin correction (reduces ΔfCO_2 by ~2 µatm; Woolf et al., 2016) is negligible relative to the observed ΔfCO_2 and was therefore ignored. K_{660} from the DT experiment is summarized in Appendix A2. The EC dataset offers high temporal resolution (~10 min), enabling investigation of small-scale processes influencing gas exchange. The EC observations span a broad range of wind speeds (1 to 12 m s^{-1}, Fig. 4A), providing a robust constraint of K_{660_CO2} under low-to-moderate wind conditions. In contrast, DT-derived K_{660} represents daily averages, in which short-term extremes (i.e., low and high wind conditions) are

https://doi.org/10.5194/egusphere-2025-6095
Preprint. Discussion started: 19 January 2026

223 smoothed, resulting in seven observations concentrated at U_{10N} of 5-9 m s^{-1} (Fig. 4A). Within this
224 wind range, DT-and EC-derived K_{660} values agree well (Fig. 4).

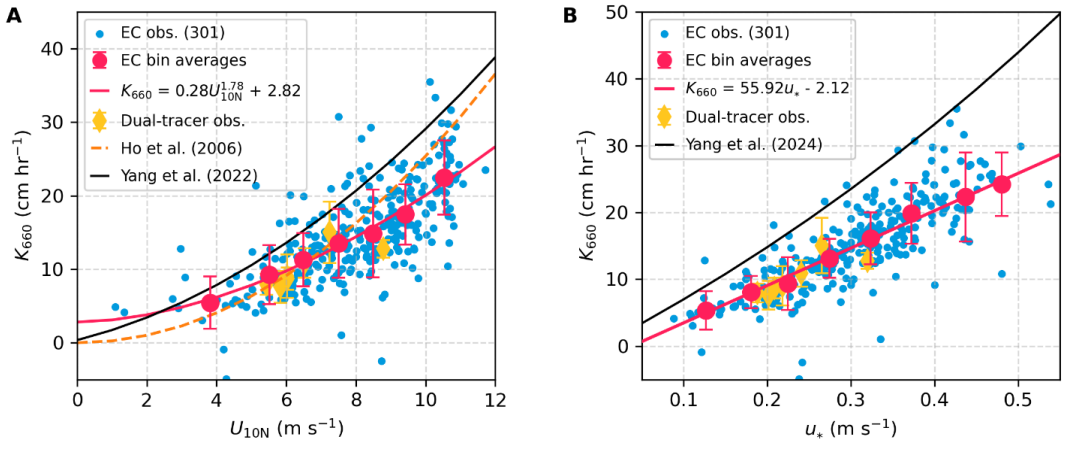

225

226 **Figure 4: Gas transfer velocity (K_{660_CO2}) in the central Baltic Sea during the CenBASE cruise. A**:
227 Relationships between K_{660} and U_{10N}. **B**: Relationships between K_{660} and observed u_*. Blue dots in both
228 panels represent 10-min K_{660_CO2} (N = 301), with red dots denoting bin averages (1 m s^{-1} U_{10N} bins or 0.05
229 m s^{-1} u_* bins) ± 1 STD. Red lines indicate fit to the bins, with R^2 of 0.48 for the fit with U_{10N} and 0.59 with
230 u_*. Yellow diamonds show dual-tracer (DT) transfer velocities ($K_{660\_3He/SF6}$) measured concurrently with EC
231 (Dobashi et al., submitted). The orange line in panel A denotes the open ocean DT-based parameterisation
232 from Ho et al. (2006). The black lines in panels A and B correspond to the open-ocean EC-based
233 parameterizations of Yang et al. (2022; U_{10N}-dependent) and Yang et al. (2024; u_* and sea-state dependent),
234 respectively.

235

236 DT-derived K_{660} values during CenBASE also mostly match the open-ocean DT-based
237 parameterization of Ho et al. (2006) under equivalent wind speeds (orange dashed line in Fig. 4A).
238 However, EC-derived K_{660_CO2} values deviate systematically from this open-ocean relationship
239 (Ho et al., 2006), being higher at low wind speeds (1-7 m s^{-1}, +12%) and lower at high wind speeds
240 (7-12 m s^{-1}, -18%) (Fig. 4A). This divergence does not contradict the agreement between the DT-
241 and EC-based K_{660} observations, as this agreement falls within the 5-9 m s^{-1} range (where the DT
242 data concentrate). Fitting K_{660_CO2} with U_{10N} reveals a weaker wind speed dependence than the
243 open sea DT-based parameterisation (Fig. 4A). It is worth noting that including a constant term in
244 the K_{660_CO2}-U_{10N} fitting function (i.e., $K_{660\_CO2} = aU_{10N}^{b} + c$, R^2 = 0.48) improves the fit

https://doi.org/10.5194/egusphere-2025-6095
Preprint. Discussion started: 19 January 2026

compared to a purely power-law form (i.e., $K_{660\_CO2} = aU_{10N}^{b}$, R^2 = 0.42) (Fig. A5), suggesting a non-zero CO_2 exchange (~3 cm hr^{-1}) under calm conditions. This is unsurprising since the chemical enhancement (Cole & Caraco, 1998; Fairall et al., 2022) and likely buoyancy flux sustain CO_2 transfer at low winds (McGillis et al., 2004; Wanninkhof et al., 2009).

Notably, the DT data collected during CenBASE provide only limited constraints at wind speeds below 5 m s^{-1} and above 9 m s^{-1}, and the K_{660}-U_{10N} relationship derived from these data is sensitive to the chosen functional form (Fig. A5). Moreover, the DT-based open ocean K_{660} estimates are lower than the EC CO_2-based estimates over the wind speed range observed during CenBASE (Fig. 4A), likely reflecting differences in methodology. Because the CenBASE DT data have been interpreted in detail by Dobashi et al. (submitted), and, more importantly, because the EC measurements resolve finer-scale processes and ensure methodological consistency, the subsequent section focuses on comparing EC CO_2 observations in the Baltic Sea with the EC CO_2 observations in the open ocean.

3.4 Suppression of air-sea CO_2 exchange

The EC-derived K_{660_CO2} during CenBASE was generally lower than open-ocean EC CO_2 transfer velocities (Yang et al., 2022; 2024) (Figs. 4A and 4B), indicating a substantial suppression of CO_2 exchange in the Baltic Sea. To explain this reduction, we partition the total gas transfer velocity (K_{660}) into interfacial (K_{i660}) and bubble-mediated (K_{b660}) components (i.e., $K_{660} = K_{i660} + K_{b660}$). K_{i660} is primarily driven by wind stress or u_*, whereas K_b depends on both the wind forcing and sea state. A machine-learning analysis of 15 open ocean datasets identified the significant wave height (H_s, including both windsea and swell) as a key proxy for sea state that strongly affects K_{660_CO2} (Yang et al., 2024). Following this separation framework and the open ocean EC data analysis (Yang et al., 2024), the K_{660} can be expressed as (Fig. 4B, black line):

$$K_{660} = K_{i660} + K_{b660} = 55u_* + 10u_*H_s \quad (3)$$

Because K_b depends on solubility, normalizing it using the Schmidt number (i.e., converting K_b to K_{b660}) may not be strictly appropriate. However, the sensitivities of the CO_2 transfer velocity to $Sc^{-1/2}$ and α^{-1} are nearly identical (see Fig. A1 in Dong et al., 2025). Therefore, normalization using either Sc or α produces almost the same gas transfer velocities. For simplicity and consistency, we adopt the Sc-based normalization in this study. Applying Equation 3 to the equivalent wind speeds

https://doi.org/10.5194/egusphere-2025-6095
Preprint. Discussion started: 19 January 2026

observed during CenBASE yields on average values of K_{i660} = 15.1 cm hr^{-1}, K_{b660} = 7.0 cm hr^{-1}, and K_{660} = 22.1 cm hr^{-1}. In contrast, the observed EC K_{660} during CenBASE was on average 14.9 cm hr^{-1}, 33% (7.2 cm hr^{-1}) lower than the open ocean K_{660} estimate (i.e., 22.1 cm hr^{-1}).

Equation 3 implies a linear dependence of K_{660_CO2} on u_*. Regression of the observed K_{660_CO2} against u_* indeed yields an approximately linear relationship (Fig. 4B), consistent with prior findings at low-to-moderate winds (Landwehr et al., 2018; Yang et al., 2022). Additionally, the K_{660_CO2}-u_* fit (R^2 = 0.59) outperforms the K_{660_CO2}-U_{10N} fit (R^2 = 0.48), confirming that u_* better captures variability in gas transfer velocity than U_{10N} (Jähne et al., 1987; Landwehr et al., 2018; Yang et al., 2022). As shown in Fig. 3A, the observed u_* during CenBASE was ~10% higher than open-ocean values under equivalent wind speeds, implying a ~10% enhancement in K_{660_CO2} due to fetch-related increases in shear stress (Vickers and Mahrt, 1997). It is important to note that the observed 33% reduction in K_{660_CO2} includes this enhancement, suggesting that CO_2 exchange was suppressed even more, by ~43% (9.2 cm h^{-1}) relative to open-ocean conditions.

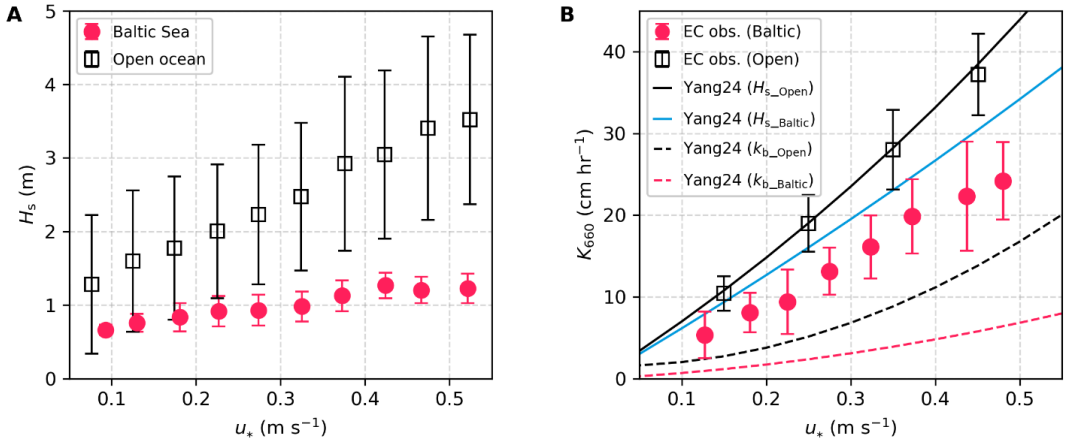

Figure 5: Comparison of significant wave height (H_s) and K_{660_CO2} between the Baltic Sea and the open ocean. A: H_s in the Baltic Sea during CenBASE (red dots) and in the open ocean (black squares), with error bars representing ± 1 STD. The data are extracted from ERA5 according to the EC cruise tracks (Yang et al., 2022). **B:** K_{660_CO2} observations in the Baltic Sea during CenBASE (red dots, the same as the red dots in Fig. 4B) and in the open ocean (black squares, Yang et al., 2022). The black solid and blue lines correspond to the parameterised K_{660_CO2} (Equation 3; Yang et al., 2024) using the open ocean and the Baltic Sea H_s, respectively. The black and red dashed lines denote the parameterized bubble-mediated transfer component (K_b; Equation 3) using the open ocean and the Baltic Sea H_s.

https://doi.org/10.5194/egusphere-2025-6095
Preprint. Discussion started: 19 January 2026

According to Equation 3, K_b is linearly dependent on H_s. Due to the limited fetch, the H_s during CenBASE was 57% lower than in the open ocean at the equivalent u_* (Fig. 5A, Table 1), and this reduction is expected to cause a comparable decrease in K_b. Using the extracted H_s values from ERA5 for CenBASE, the parameterized K_{b660} decreases on average from 7.0 cm hr^{-1} to 4.0 cm hr^{-1}, corresponding to an 18% suppression on the total K_{660_CO2} (Fig. 5B; Table 1), explaining about half of the observed suppression during CenBASE.

Surfactants inhibit both interfacial (e.g., Frew, 1997) and bubble-mediated gas exchange (e.g., Woolf, 1993), and their concentrations in the Baltic Sea are substantially higher than in the open ocean. We assume that all residual suppression of K_{660_CO2} during CenBASE, which cannot be explained by fetch effects, is caused by surfactants. Under this assumption, the residual 25% suppression (i.e., 5.4 cm hr^{-1}; Fig. 5B and Table 1) reflects the impact of elevated surfactant levels. This effect is not captured by the Yang et al. (2024) parameterization, which is based primarily on open-ocean observations characterized by low surfactant concentrations (Wurl et al., 2011; Fig. A6).

The resulting suppression fraction (*sf*) is consistent in magnitude with previous field-based estimates (Fig. 6; Mustaffa et al., 2020; Salter et al., 2011; Yang et al., 2021) within uncertainty (see Section 3.5). The constrained *sf* is generally smaller than laboratory-derived values (Fig. 6A), likely due to challenges in extrapolating laboratory conditions to the field. Notably, previous studies report conflicting relationships between *sf* and surfactant concentration. Some show increasing *sf* with increasing concentration (Mesarchaki et al., 2015; Pereira et al., 2018; Ribas-Ribas et al., 2018), whereas others identify a threshold concentration above which *sf* shows little change (Mustaffa et al., 2020; Schmidt and Schneider, 2011) (Fig. 6A). Because surfactant concentrations were nearly constant during CenBASE, we cannot assess this relationship here.

Several studies also show that *sf* decreases with wind speed (Fig. 6B; Bock et al., 1999; Mesarchaki et al., 2015; Salter et al., 2011; Yang et al., 2021), and the *sf* constrained here aligns well with these findings, especially those from field observations. Fitting *sf* as a function of u_* yields a correction factor (i.e., 1 – *sf*) that can be applied to Equation 3 to account for surfactant effects, generating the updated parameterization:

$$K_{660} = (1 - 0.38e^{-1.25u_*})(55u_* + 10u_*H_s) \quad (4)$$

https://doi.org/10.5194/egusphere-2025-6095
Preprint. Discussion started: 19 January 2026

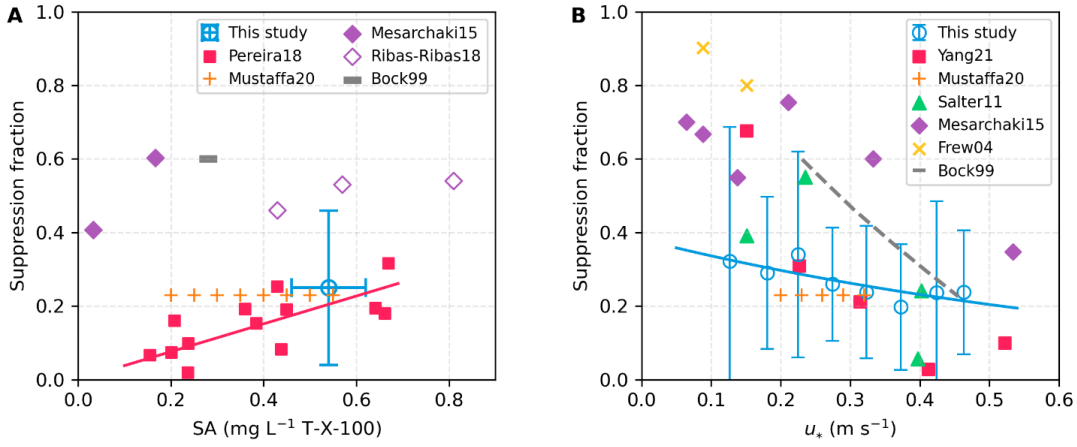

Figure 6: Surfactant-induced suppression fraction on K_{660} (*sf*) from this study and previous work. A: *sf* as a function of surfactant concentration under low-moderate wind speeds. The blue circle shows the mean constrained *sf* from this study; horizontal and vertical error bars denote the standard deviation of observed SA and the associated uncertainty of the constrained *sf*. Red squares indicate *sf* from wave-tank experiments with natural Atlantic seawater at wind speeds <13 m s^{-1} (Pereira et al., 2018), with the red line showing the linear fit (*sf* = 38×SA). Orange pluses show *sf* constrained from field K_{660} observations using the chamber technique with natural surfactant (Mustaffa et al., 2020). Diamonds (filled/unfilled) and the grey dash represent wave-tank studies using artificial soluble surfactants (Mesarchaki et al., 2015; Ribas-Ribas et al., 2018; Bock et al., 1999). **B**: *sf* as a function of u_*. Blue circles show *sf* constrained from the residual suppression of observed K_{660_CO2} from this study, with error bars indicating uncertainties. The blue line corresponds to the fit based on the blue circles ($0.38\times e^{1.25u*}$, R^2 = 0.65). Red squares represent values derived from an EC-based CO_2 transfer velocity study. Orange pluses denote the Mustaffa et al. (2020) dataset with surfactant concentrations of 0.2-0.6 mg L^{-1}. Green triangles show *sf* inferred from EC-based DMS and DT exchange experiments in artificial insoluble surfactant patches (Salter et al., 2011). Purple diamonds represent Mesarchaki et al. (2015), who used ~0.2 mg L^{-1} of artificial soluble surfactant. Yellow crosses indicate *sf* derived from coastal heat transfer measurements (Frew et al., 2004). The grey dashed line shows laboratory experiments with artificial soluble surfactants at ~0.3 mg L^{-1} (Bock et al., 1999).

This parameterization reflects conditions during CenBASE, where the surfactant concentration was relatively stable at ~0.5 mg L^{-1}. If a SA concentration-dependent *sf* is needed, one option is the published linear relationship $sf = 0.32SA + 0.025$ (Pereira et al., 2018). However, this formulation is physically inconsistent because it predicts a non-zero suppression even when SA =

https://doi.org/10.5194/egusphere-2025-6095
Preprint. Discussion started: 19 January 2026

0, whereas *sf* should theoretically approach zero in surfactant-free conditions. To address this, we re-evaluated the same dataset used in the original study (Pereira et al., 2018) and fitted a proportional relationship that passes through the origin: $sf = 0.38SA$. The goodness of fit (R^2 = 0.49) is only marginally lower than the original relationship (0.51, Pereira et al., 2018), indicating that the proportional form captures the data nearly as well while remaining physically realistic. For the mean CenBASE surfactant concentration (SA = 0.54 mg L^{-1}), this relationship yields $sf = 0.21$. Applying this SA-dependent suppression to the wind-dependent correction in Equation 4 results in the combined parameterization:

$$K_{660} = \frac{1-0.38SA}{0.79}(1 - 0.38e^{-1.25u_*})(55u_* + 10u_*H_s) \quad (5)$$

Previous studies have suggested that water-side convection may influence gas exchange in both open-ocean (McGillis et al., 2004) and Baltic conditions (Rutgersson and Smedman, 2010). During CenBASE, a small spar buoy recorded oxygen, temperature, and salinity at depths of 1.2 m and 2.9 m. Dissolved oxygen exhibited small-scale variability with similar patterns at both depths (Fig. A7), indicating coherent near-surface structure over 5-20 m scales, likely driven by wind-induced turbulence intermittently exposing surface patches to the atmosphere. In contrast, no corresponding variability was observed in temperature or salinity (Fig. A7), suggesting that convection played a negligible role in gas exchange under the observed conditions. This supports our assumption that the deviation of the K_{660_CO2} between the Baltic Sea and the open ocean can be fully attributed to the combined effects of the limited fetch and the elevated surfactants.

3.5 Uncertainty analysis

The quantification results shown above are not free from uncertainty. First, we use the $K_b \propto u_* H_s$ relationship for the bubble component, which fits best with the EC-based K_{660_CO2} observations (Yang et al., 2024). However, alternative formulations have been proposed, such as $K_b \propto u_*^{1.67} H_s^{0.67}$ (Deike and Melville, 2018) and $K_b \propto u_*^{0.9} H_s^{0.9}$ (Brumer et al., 2017a; Fairall et al., 2022). These different exponents indicate that the relative contributions of u_* and H_s to gas exchange may vary slightly, introducing parameterization uncertainty. Considering both observational and fitting uncertainties, we assign a 20% uncertainty to the parameterization of Equation 3 (Yang et al., 2024). This uncertainty propagates through the suppression estimates. For instance, the uncertainty in the u_*-related K enhancement estimate is approximately 0.4 cm hr^{-1} (i.e., 2.2 cm hr^{-1} × 20%).

https://doi.org/10.5194/egusphere-2025-6095
Preprint. Discussion started: 19 January 2026

The suppression analysis uses H_s data derived from ERA reanalysis, which likely carry an uncertainty of about 30% in the Baltic Sea (Giudici et al., 2023). Consequently, the uncertainty in the H_s-related suppression estimate is ~1.4 cm hr^{-1} (i.e., $\sqrt{(4.0 \times 20\%)^2 + (4.0 \times 30\%)^2}$ cm hr^{-1}). The uncertainty associated with the surfactant-related suppression is substantially larger because it is not directly determined but inferred as a residual after accounting for other components. Combining the propagated uncertainties from the parameterised total K and from two fetch-induced suppression estimates yields an uncertainty of 4.5 cm hr^{-1} (i.e., $\sqrt{(22.1 \times 20\%)^2 + 0.4^2 + 1.4^2}$ cm hr^{-1}), corresponding to approximately 85% of the estimated suppression value (Table 1).

Table 1. Comparison of mean gas transfer velocities between measurements in the Baltic Sea and estimates using the open ocean parameterisation from Yang et al. (2024) under identical wind speed conditions. The percentages in parentheses in the K_i, K_b, and K columns indicate the relative difference between the Baltic Sea and the open ocean. The last column is the uncertainty assessment of the values in the K column with the values in parentheses representing the relative uncertainties. The positive (negative) sign represents the enhancement (suppression).

Gas transfer velocity (cm hr^{-1})			K_{i660}	K_{b660}	K_{660}	Uncertainty
Open ocean			15.1	7.0	22.1	± 4.4 (± 20%)
Impact factors	Fetch	u_*	+1.5 (+10%)	+0.7 (+10%)	+2.2 (+10%)	± 0.4 (± 20%)
		H_s	0	-4.0 (-57%)	-4.0 (-18%)	± 1.4 (± 36%)
	Surfactants		Unsure	Unsure	-5.4 (-25%)	± 4.6 (± 85%)
Baltic Sea (CenBASE)			-	-	14.9 (-33%)	-

3.6 Implications for Baltic Sea CO_2 flux estimates

The CenBASE cruise took place during the summer bloom (July), when chlorophyll-*a* (Chl-*a*) is high (Pitarch et al., 2016) and fCO_{2w} is strongly reduced by primary productivity (Bittig et al., 2024). To upscale these results, we examine how fetch and surfactants shape the climatological CO_2 flux of the Baltic Sea. The fCO_{2w} indicates a CO_2 sink in summer and a source in winter (Fig. 7A). However, weaker summer winds and stronger winter winds suggest that the magnitudes of uptake and outgassing may be similar. Seasonal cycles of u_* and H_s closely follow wind speed (Fig.

https://doi.org/10.5194/egusphere-2025-6095
Preprint. Discussion started: 19 January 2026

7B), while chlorophyll-*a* (Chl-*a*) peaks during the spring-summer bloom and remains low in winter (Fig. 7C). We estimate monthly surfactant concentrations by scaling the July CenBASE value (0.54 mg L^{-1}) with monthly chlorophyll-*a* concentrations following the idea of Wurl et al. (2011) and using the formula 0.54×Chl-*a*/Chl-$a_{\_July}$ mg L^{-1}. Equation 5 is then used to compute the corresponding suppression of gas transfer, $1-\frac{1-0.38SA}{0.79}(1-0.38e^{-1.25u_*})$. The resulting *sf* reflects the seasonal chlorophyll-*a* cycle and modulations by u_*, yielding ~25% suppression in summer and ~10% in winter (Fig. 7C). However, surfactant concentrations are not solely determined by chlorophyll-a; for example, humic acids also act as surfactants (e.g., Klavins & Purmalis, 2010), and the Baltic Sea is known for elevated humic acid levels due to significant terrestrial inputs (Hammer et al., 2017). Therefore, estimating surfactants based solely on chlorophyll-*a* has inherent limitations.

We estimate K_{660} using three parameterization schemes: the conventional open ocean DT-based U_{10N} formulation (Ho et al., 2006), the open ocean EC CO_2-based u_*-H_s formulation (Equation 3; Yang et al., 2024), and the Baltic Sea EC CO_2-based u_*-H_s-SA formulation (Equation 5). Although all these schemes reproduce similar seasonal patterns, their magnitudes differ (Fig. 7D), reflecting sea state and surfactant effects as well as the methodological differences. The u_*-H_s-SA parameterization yields lower values than the u_*-H_s scheme because it incorporates surfactant-induced suppression from the surfactant. This suppression is especially stronger in summer when SA concentrations are highest, leading to largest discrepancies of the estimated climatological K_{660} from the u_*-H_s-SA and the u_*-H_s schemes. As shown in Section 3.4, K_{660} during CenBASE has been reduced by 33%. Notably, this reduction is relative to the open ocean EC-based estimates. When compare with the open ocean DT-based U_{10N} formulation, however, this reduction occurs only at wind speeds above ~7 m s^{-1}. At lower wind speeds, the EC-based K_{660} observations during CenBASE exceed the DT-based estimates (Fig. 4A). Because climatological Baltic Sea wind speeds are typically below 7 m s^{-1} in Spring, Summer, and Autumn (Fig. 7A), the u_*-H_s-SA parameterization produces higher K_{660} than the U_{10N} formulation in these seasons. In winter, despite higher wind speeds, the u_*-H_s-SA scheme still exceeds the U_{10N}-based estimates due to the modulation of the surfactants. The SA concentration in winter is estimated to be three times lower than during summer CenBASE cruise (Fig. 7C), resulting in much weaker suppression.

https://doi.org/10.5194/egusphere-2025-6095
Preprint. Discussion started: 19 January 2026

Overall, relative to the conventional U_{10N} formulation (Ho et al., 2006), the u_*-H_s-SA parameterization increases K_{660} in all seasons, enhancing both summer CO_2 uptake by ~10% and winter outgassing by ~30%, and amplifying the seasonal cycle by ~40%. These opposing seasonal effects are expected to largely compensate, resulting in only a modest change in the annual mean CO_2 flux.

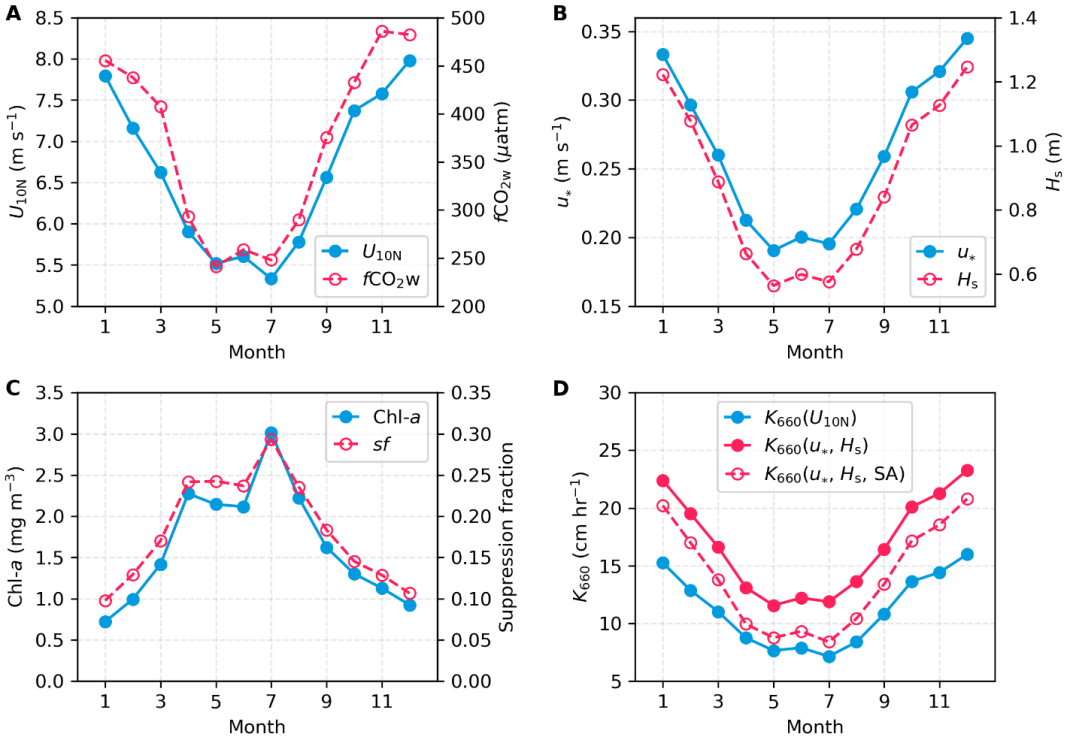

Figure 7: Climatological seasonal variations of environmental variables and gas transfer velocities in the Baltic Sea. A: U_{10N} (blue) and fCO_{2w} (red; Bittig et al., 2024). **B**: u_* (blue) and H_s (red). U_{10N}, u_*, and H_s are averaged from the ERA5 monthly reanalysis data product (Hersbach et al., 2020) for 1998-2018. **C**: Surfactant concentrations scaled from monthly chlorophyll a (Pitarch et al., 2016) and surfactant-induced suppression fraction of K_{660} based on the SA- and U_{10}-dependent parameterisation (Equation 5). **D**: K_{660} estimated from different parameterizations: U_{10N}-based (blue; Ho et al., 2006), u_*-H_s-based (red solid; Equation 3, Yang et al., 2024); u_*-H_s-SA-based (red dashed; Equation 5).

https://doi.org/10.5194/egusphere-2025-6095
Preprint. Discussion started: 19 January 2026

4 Discussion and conclusions

A robust understanding of air-sea gas exchange mechanisms is fundamental for accurately quantifying CO_2 fluxes, which is essential for accurate carbon budgets and climate projections. Most previous studies have focused on the open ocean, where K_{660} is typically parameterized as a function of wind speed. In contrast, marginal seas such as the Baltic Sea exhibit more complex dynamics due to limited fetch and abundant surfactants, which modulate the wind speed dependence of gas exchange. To investigate these processes, a dedicated experiment was conducted in the central Baltic Sea during the CenBASE cruise, employing two commonly used techniques: eddy covariance and dual-tracer methods. The K_{660} derived from both techniques agrees well, confirming the reliability of both methods for gas transfer velocity observations. The observed CO_2 transfer velocity shows a significant reduction compared to the open-ocean CO_2 observations and parameterizations under comparable wind conditions (Yang et al., 2024; Fig. 4). This reduction can be attributed to three competing processes (summarized in Fig. 8): 1) a 10% enhancement from fetch-limited increases in friction velocity, 2) an 18% suppression from reduced significant wave height, and 3) a 25% suppression from elevated surfactant concentrations. Together, these effects explain the overall 33% reduction in CO_2 exchange during CenBASE relative to the EC-based open ocean K_{660_CO2}.

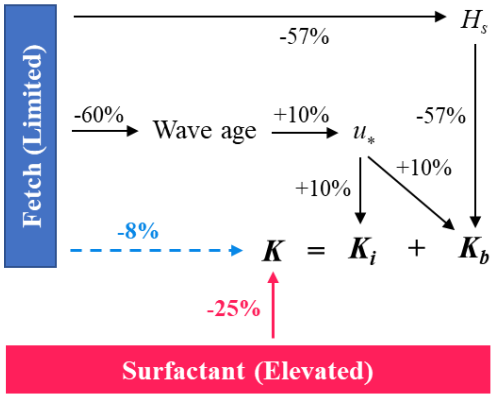

Figure 8: Schematic illustrating how fetch and surfactants modulate the CO_2 transfer velocity (K) in the Baltic Sea relative to the open ocean. Values denote the relative magnitude of enhancement (+) or suppression (–) for each process (Table 1). Black arrows and their associated values indicate the effect of

https://doi.org/10.5194/egusphere-2025-6095
Preprint. Discussion started: 19 January 2026

fetch on individual gas exchange components, while the blue value on the dashed arrow shows the net fetch effect on total *K*. The red value and arrow represent the constrained surfactant-induced suppression of *K*.

During CenBASE, fetch lengths ranged from 50-300 km, in contrast to more than 1000 km in the open ocean. The limited fetch exerts both enhancing and suppressing effects on gas exchange in the Baltic Sea (Fig. 8). Shorter fetch produces a younger wave field dominated by shorter and steeper waves, increasing surface roughness and thereby enhancing u_* and K_{660}. At the same time, limited fetch constrains wave development, leading to a ~60% reduction in H_s (Fig. 5A). As a key proxy for wave-breaking intensity (Brumer et al., 2017; Deike, 2021; Zhao et al., 2003), reduction in H_s diminishes wave breaking and consequently suppresses bubble-mediated gas transfer (Dobashi & Ho, 2023; Fairall et al., 2006; Ocampo-Torres & Donelan, 1995; Woolf, 2005). These findings emphasize the need to incorporate sea-state dependence into K_{660} parameterizations (Brumer, 2017; Deike & Melville, 2018; Fairall et al., 2022; Yang et al., 2024). When direct wave observations are unavailable, reanalysis products (e.g., ERA5; Hersbach et al., 2020) can serve as a first-order estimate of wave conditions for *K* evaluation (Bessonova et al., 2025; Giudici et al., 2023).

Although bubble effects are expected to be stronger for low-solubility tracers such as ^{3}He and SF_6 than for CO_2, the EC CO_2-derived and dual-tracer-derived K_{660} values agreed closely (Fig. 4A). This is primarily because the bubble contribution to the total gas exchange during CenBASE was relatively small due to the low wind regime (Fig. 5B). According to the widely used model (Woolf, 1997), bubble-mediated transfer contributes ~25% to total CO_2 exchange and ~35% to ^{3}He/SF_3 exchange under wind speeds of 0-12 m s^{-1}. This difference corresponds to only ~1.5 cm hr^{-1} higher K_{660} for dual tracers, which lies well within the measurement uncertainty and is therefore not practically distinguishable. Moreover, the much lower salinity in the Baltic Sea further limits the bubble-induced solubility dependence of *K*. Although the bubble size observations with the bubble buoy did not work during CenBASE, it is well established that bubbles coalesce easily in fresh water (this is inhibited in salt water), so the initial bubble size distribution in fresher water quickly evolves towards larger bubbles through coalescence (e.g., De Leeuw et al., 2011). This coalescence effect has little influence on the gas transfer of moderately soluble gases such as CO_2 but reduces K_b for very low-solubility gases (e.g., ^{3}He and SF_6) due to the reduction of bubble surface area,

https://doi.org/10.5194/egusphere-2025-6095
Preprint. Discussion started: 19 January 2026

thereby narrowing the difference in K_{b660} between CO_2 and the $^3He/SF_6$. This also indicates that the parameterization of the bubble-mediated component derived from open-ocean EC data (Yang et al., 2024) remains applicable to the Baltic Sea, despite differences in salinity and thereby bubble size distribution.

The suppression of gas exchange by surfactants has been well documented in laboratory studies, which report 10-65% reductions in K depending on surfactant concentration (Bock et al., 1999; Frew et al., 1990; Goldman et al., 1988; Mesarchaki et al., 2015; Pereira et al., 2016; Pereira et al., 2018; Ribas-Ribas et al., 2018; Schmidt & Schneider, 2011). Based on the empirical relationship derived by Pereira et al. (2018) using laboratory data, the CenBASE microlayer surfactant concentration (0.54 ± 0.08 mg L^{-1}) corresponds to an estimated ~20% reduction in K. Field studies have reported similar magnitudes of suppression (24-55%) under artificial surfactant additions (Brockmann et al., 1982; Salter et al., 2011). More recently, field chamber measurements indicate ~23% suppression for natural surfactant levels exceeding 0.2 mg L^{-1} (Mustaffa et al., 2020), and EC-based K_{660_CO2} observations have shown ~30% suppression at moderate winds (~7 m s^{-1}) under likely high surfactant conditions (Yang et al., 2021). Thus, the 25% suppression estimated in this study agrees well with previous laboratory and field results.

Our findings refine the mechanistic understanding of air-sea gas exchange and have important implications for coastal CO_2 flux estimates. Using the u_*-H_s-SA parameterization, both summer uptake and winter outgassing of CO_2 in the Baltic Sea increase compared to a conventional U_{10N}-based parameterization, amplifying the seasonal cycle. Because many coastal regions exhibit similarly short fetch and elevated surfactant concentrations (Fig. A6), the mechanism-based parameterization proposed here is expected to yield systematically different gas exchange efficiencies than conventional wind speed-based formulations. The mechanism-based K parameterization could alter coastal CO_2 flux estimates (e.g., Resplandy et al., 2024), influencing annual means, long-term trends, seasonal cycles, and spatial patterns. An improved estimate of the ocean CO_2 sink may also help reduce discrepancies between the data-based and model-based global carbon budgets (Friedlingstein et al., 2025). The improvement in the estimate of K is especially important for mCDR studies, which are often tested or developed in coastal environments (e.g., Ho et al., 2024). Beyond CO_2, the updated parameterization may also apply to other greenhouse gases, such as N_2O, which shares the same interfacial exchange mechanism and

https://doi.org/10.5194/egusphere-2025-6095
Preprint. Discussion started: 19 January 2026

exhibits similar bubble-mediated behavior due to comparable solubility. Application to DMS is also possible, provided the bubble-mediated component is omitted.

Despite the advances from the CenBASE campaign, several uncertainties remain. The surfactant-induced suppression was inferred from residual differences between Baltic Sea and open-ocean K_{660_CO2} after correcting for fetch effects, and therefore carries considerable uncertainty even though the magnitude is consistent with previous field constraints. We were unable to partition the surfactant-induced suppression between interfacial and bubble-mediated pathways because available evidence is insufficient to quantify their relative roles. Observations were limited to low-to-moderate wind speeds (<12 m s^{-1}), preventing evaluation of the surfactant effect under high wind speed conditions. Furthermore, surfactant concentrations were relatively uniform during CenBASE, so suppression could not be assessed across natural SA concentration gradients. Given the strong seasonal and spatial variability in biological production, the transferability of our quantified suppression values beyond the CenBASE conditions is uncertain. Addressing these limitations will require coordinated, multi-season observations across diverse fetch conditions, surfactant regimes, and wind speeds. Such efforts are essential for building a generalizable framework for gas exchange in marginal seas and for improving both regional CO_2 budgets and assessment of emerging mCDR applications.

https://doi.org/10.5194/egusphere-2025-6095
Preprint. Discussion started: 19 January 2026

Appendix

A1. Dual-tracer experiments

The *K* was also determined using the $^3He/SF_6$ dual tracer technique. ^3He and SF_6 were injected into the surface ocean, and their concentrations were monitored over time. Assuming that air-sea gas exchange is the only process affecting the $^3He/SF_6$ ratio, *K* can be derived from the temporal change in their ratio. The two tracers, ^3He and SF_6, were injected with a molar ratio of 1:340 on 6 July 2022 at ~7 m depth for 40 minutes, centered at 57.263°N, 20.147°E. The injected tracers were then tracked using an underway SF_6 analysis system (Ho et al., 2002), which continuously measures the SF_6 concentration at the water surface, and the vessel-mounted acoustic Doppler current profiler (ADCP) (150 kHz Ocean Surveyor, RD Instruments).

Near the center of the patch of injected tracers, water samples were taken using the CTD rosette equipped with 13 5-L Niskin bottles. Discrete SF_6 samples were taken from the Niskin bottles using 250-ml syringes. The SF_6 concentration was measured onboard the ship using a gas chromatograph equipped with an electron capture detector (GC-ECD) in combination with a purge-and-trap system (Bullister and Weiss, 1988; Gerke et al., 2024). About 40 ml of seawater for discrete ^3He samples was collected in copper tubes placed in aluminum channels, with both ends sealed by stainless steel clamps. The ^3He samples were sent to the laboratory at the Institute of Environmental Physics at the University of Bremen after the cruise. At the laboratory, ^3He was analyzed using a helium isotope mass spectrometer (MAP 215-50) (Sültenfuß et al., 2009).

A2. Surfactant sampling

Surfactant samples from the SML were collected from a small workboat positioned ~500 m upwind of the research vessel. The SML was sampled using the glass-plate technique and transferred into amber borosilicate glass bottles (Cunliffe and Wurl, 2014; Harvey and Burzell, 1972). When weather conditions were unfavorable, SML sampling was conducted from the bow of the research vessel using a Garrett screen. For surfactant samples, 18 mL SML samples were transferred into acid-washed and pre-combusted (500 °C, 8 h) 20 mL glass vials and immediately frozen at −20 °C. Surface activity was analyzed within less than one year of collection by phase-sensitive alternating-current voltammetry using a 797 VA Computrace polarograph (Metrohm, Switzerland), following Cosović & Vojvodić (1982).

https://doi.org/10.5194/egusphere-2025-6095
Preprint. Discussion started: 19 January 2026

A3. Wind speed distortion correction

During CenBASE, wind speed was measured using two instruments: a 2D sonic anemometer mounted on the ship's foremast (~17 m above MSL) and a 3D EC sonic anemometer on the front tower (~14 m above MSL) (Fig. 1). The foremast measurements are expected to be less distorted because of the higher position of the sensor (O'Sullivan et al., 2013) and are, therefore, used in this study. Nevertheless, previous work shows that the foremast-mounted anemometers can still be biased when the wind is not bow-on (e.g., Landwehr et al., 2018). To address this, we follow Landwehr et al. (2020) and use ERA5 reanalysis wind speeds, which are not affected by ship-relative flow distortions, to correct the ship measurements.

Because ERA5 winds may contain regional biases, we first calibrate ERA5 using in situ measurements from the Östergarnsholm station (Rutgersson et al., 2020). Winds from five measurement heights (normalized to U_{10}) are highly consistent, supporting the robustness of the station record (Fig. A8). We then compare station winds with ERA5 winds extracted at the station location for the period March-December 2024. To avoid land contamination, only winds from the open sector (80°-160°; Rutgersson et al., 2020) are used. ERA5 is slightly lower than the station wind below 6 m s^{-1} but higher at stronger winds (Fig. A8). Two linear regressions are applied to ERA5, resulting in good agreement with the station winds (Fig. A8). Although the ERA5 wave data used in this study are simulated by a wave model forced with ERA5 winds, which may contain minor biases, these are not expected to substantially affect the simulated wave fields (Durrant et al., 2013).

The corrected ERA5 winds are then extracted at the CenBASE cruise location and time to serve as a reference for correcting ship wind distortions. The ratio of ship to corrected ERA5 wind speed as a function of relative wind direction shows the expected distortion pattern (Fig. A9; Moat et al., 2006; B. Moat & Yelland, 2015). We fit this ratio using three functions according to the relative wind direction: (1) quadratic for -30° to 45°, (2) linear for -90° to -30°, and (3) linear for 45° to 90° (Fig. A9). This fitted relationship is used to correct the ship's wind speed. After correction, the ratio of ship to ERA5 wind speeds aligns closely with unity (Fig. A9).

https://doi.org/10.5194/egusphere-2025-6095
Preprint. Discussion started: 19 January 2026

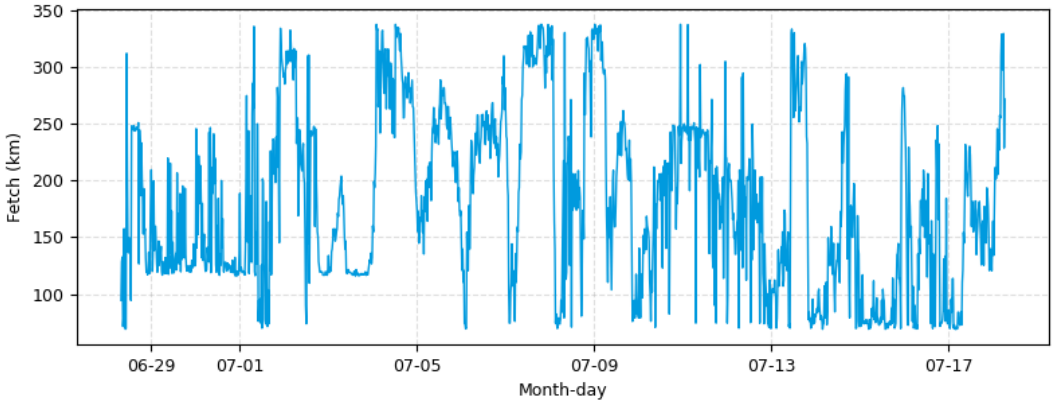

601

602 **Figure A1: Fetch of the location according to the CenBASE cruise track.** It is estimated based on the
603 length to the land and the wind direction.

604

605

https://doi.org/10.5194/egusphere-2025-6095
Preprint. Discussion started: 19 January 2026

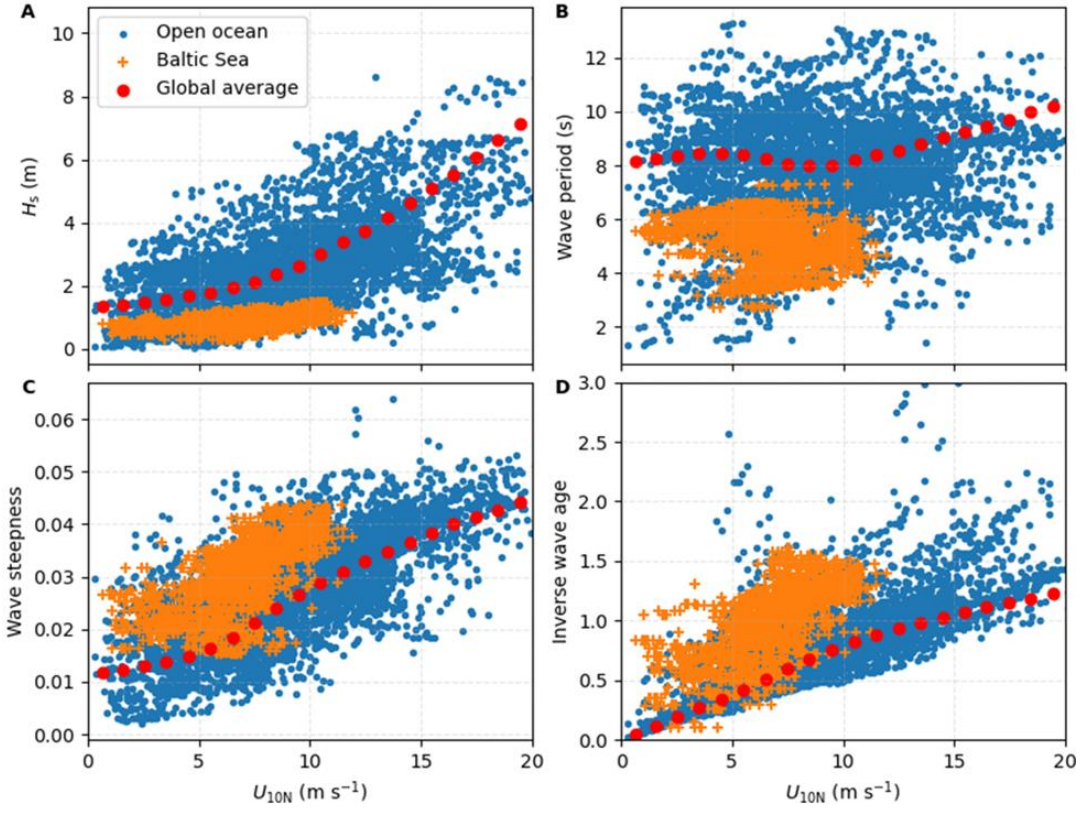

606

607 **Figure A2: Wave properties versus wind speed.** Orange: Waves in the Baltic Sea during CenBASE; Blue:
608 Waves in open ocean cruises with eddy covariance measurements (see Yang et al., 2022); and Red: Waves
609 in the global ocean average. For the global ocean average, we use the year 2024 as an example and take the
610 first day of each month at 00:00 to capture the seasonal variability. **A**: Significant wave height; **B**: Wave
611 period; **C**: Wave steepness; **D**: Inverse wave age. See the Method section 2.3 for the wave data extraction
612 information.

613

614

https://doi.org/10.5194/egusphere-2025-6095
Preprint. Discussion started: 19 January 2026

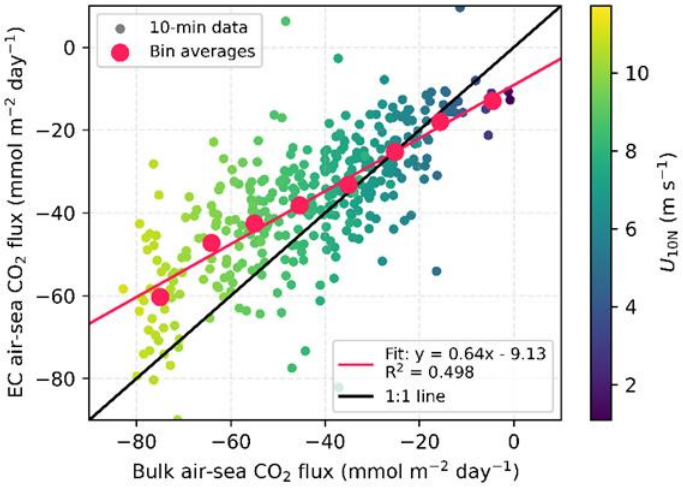

Figure A3: Bulk air-sea CO_2 flux estimates versus EC air-sea CO_2 flux observations. The Ho et al. (2006) parameterisation is used for the bulk flux estimate. The small dots are 10-minute flux data, with the large red dots representing the bin averages per 10 mmol m^{-2} day^{-1} flux interval. The EC flux observations are lower in magnitude than the bulk flux estimates at wind speeds higher than ~7 m s^{-1}.

https://doi.org/10.5194/egusphere-2025-6095
Preprint. Discussion started: 19 January 2026

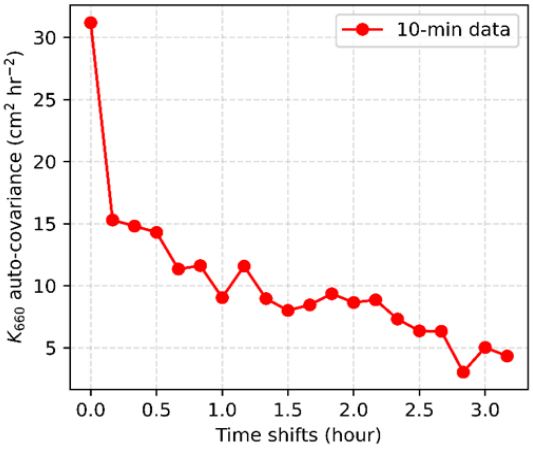

626

627 **Figure A4: Auto-covariance of EC-derived CO_2 transfer velocities (K_{660}).** The 10-min K_{660} time series
628 from 4-7 July, selected for its continuity (see Fig. 1F), was used for this analysis. The first point represents
629 the variance of the K_{660} time series, while the second point shows the covariance between the original series
630 and a version shifted by one point (i.e., 10-min). The decrease from the first to the second point indicates
631 the random uncertainty in this K_{660} time series (~50%). This uncertainty can be further reduced to ~20% for
632 a 1-hour average (i.e., $50\%/\sqrt{6}$).

633

634

635

https://doi.org/10.5194/egusphere-2025-6095
Preprint. Discussion started: 19 January 2026

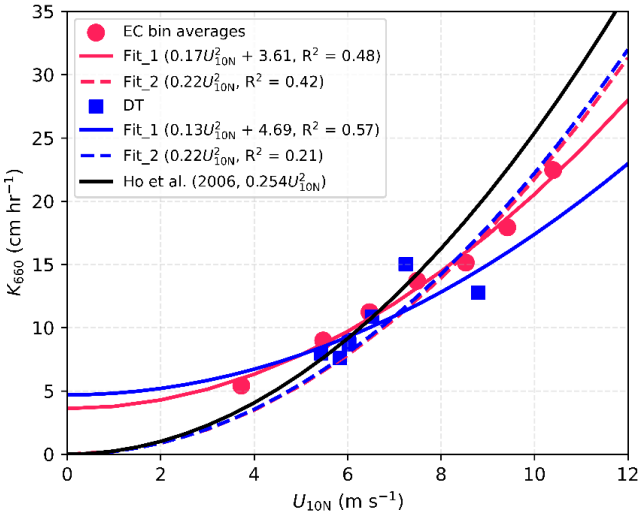

Figure A5: Observed and parameterized gas transfer velocities (K_{660}). Red dots show 10-min EC-derived bin averages (for each 1 m s^{-1} U_{10N} bin), with red lines representing parameterizations fitted to these data. Blue squares denote DT-derived K_{660} values (timescale ~1 day), with blue lines showing corresponding parameterizations. Solid lines follow the fitting form $K_{660} = aU_{10N}^2 + b$, while dashed lines follow $K_{660} = aU_{10N}^2$.

https://doi.org/10.5194/egusphere-2025-6095
Preprint. Discussion started: 19 January 2026

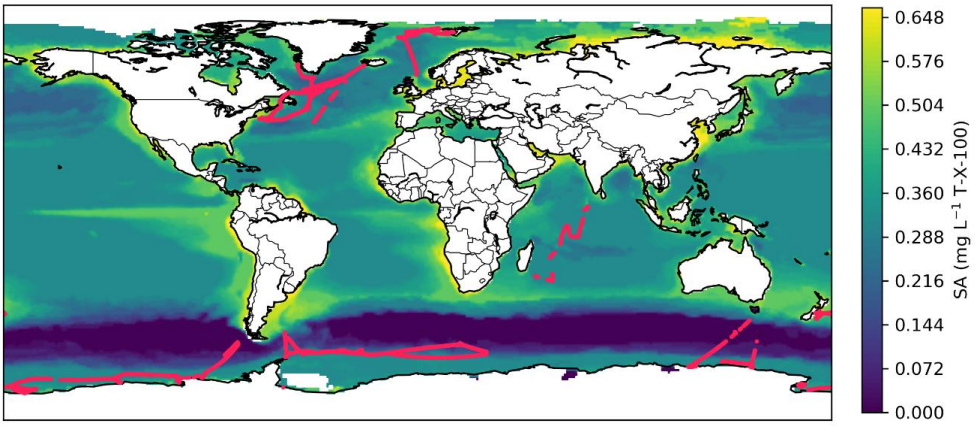

646

647 **Figure A6: Estimated surfactant distributions in the global ocean and the open ocean EC cruise**
648 **tracks.** The surfactant concentration is estimated following Wurl et al (2011) shown here as an annual mean.
649 Red lines indicate the EC cruises that were synthesized in Yang et al. (2022).

650

https://doi.org/10.5194/egusphere-2025-6095
Preprint. Discussion started: 19 January 2026

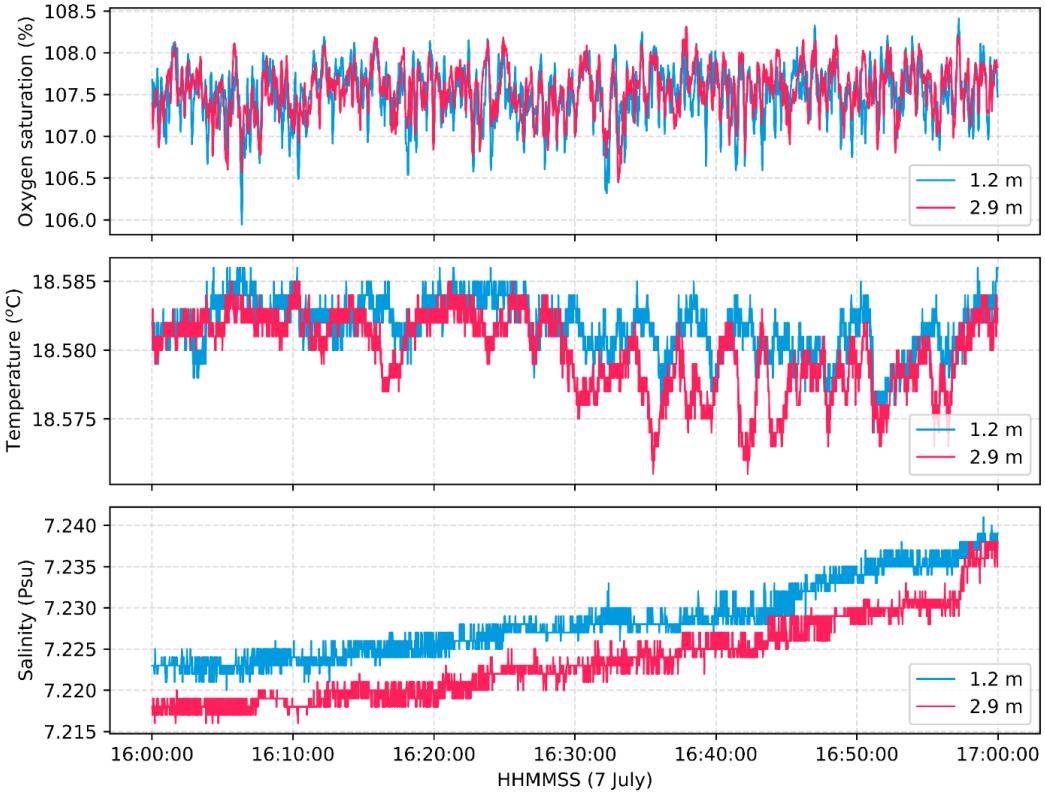

Figure A7: Representative dissolved oxygen, salinity and temperature data from the small spar buoy, showing the differences measured at 1.2m and 2.9m depth. The patterns shown here are typical of both day and night measurement periods.

https://doi.org/10.5194/egusphere-2025-6095
Preprint. Discussion started: 19 January 2026

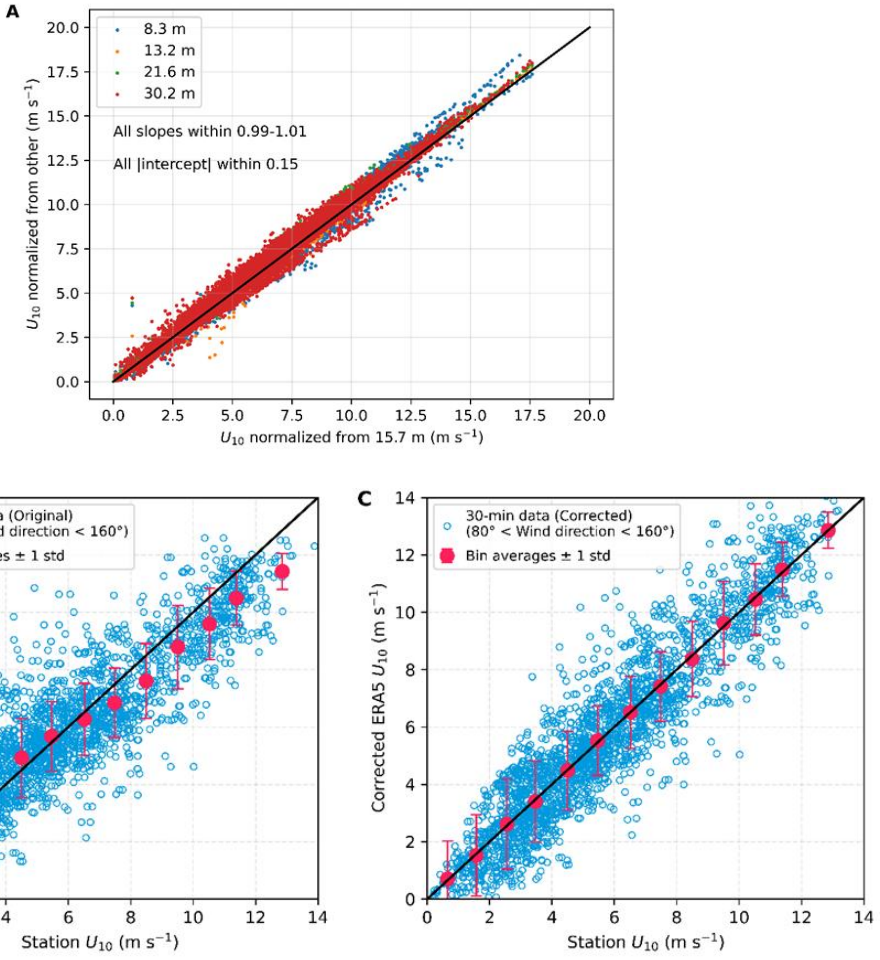

Figure A8: Correction of ERA5 wind speed using reference measurements from the Östergarnsholm station (restricted to the open sector, 80°-160°; Rutgersson et al., 2020). A: Comparison of the wind speed measurements from different heights at the Östergarnsholm station. All wind speeds were normalized to 10-meter height above MSL (U_{10}). **B:** Comparison of the station U_{10} measurements and the extracted ERA5 U_{10} at the location of the Östergarnsholm station. The red points are bin averages with error bars representing 1 standard deviation. The red points in panel B are fitted with two linear relationships: (1) $y = 0.64x + 2.05$ for station $U_{10} < 7.5$ m s^{-1}, and (2) $y = 0.88x + 0.28$ for station $U_{10} > 7.5$ m s^{-1} for correction. **C:** Comparison of the station and ERA5 U_{10} after the corrections using the relations in panel B.

https://doi.org/10.5194/egusphere-2025-6095
Preprint. Discussion started: 19 January 2026

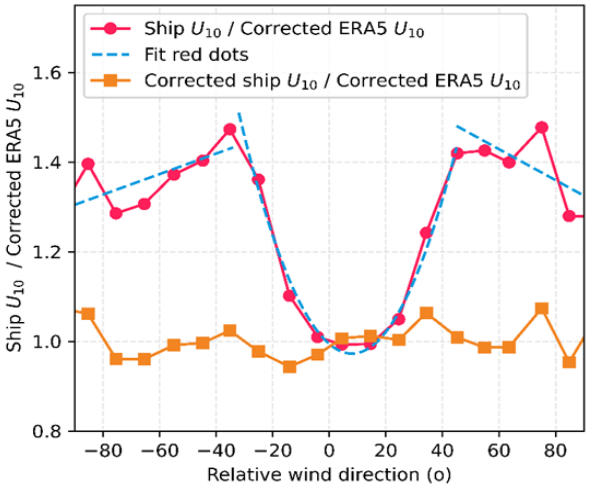

Figure A9: Ratio of ship wind speed to subsampled ERA5 wind speed before (red) and after correction (yellow) as a function of relative wind direction (RWD). ERA5 wind speeds were first calibrated against the Östergarnsholm station record (Fig. A8). The fitted relationships (blue) are: (1) y = 0.00036(RWD - 8)^2 + 0.97 for -30° to 45°, (2) y = 0.0023RWD + 1.51 for -90° to -30°, and (3) y = -0.0035RWD + 1.64 for 45° to 90°.

https://doi.org/10.5194/egusphere-2025-6095
Preprint. Discussion started: 19 January 2026

Code and data availability

The code that was used to produce the figures are available in the supplementary material. The processed 10-min EC CO_2 fluxes, wind speeds, friction velocity, and gas transfer velocity can be found in the supplementary material.

Supplement link

The link to the supplement will be included by Copernicus

Author contributions

CM, DH, AE, and GR designed the project. YD processed and analyzed the data in consultation with CM, DH, and RD. CM collected the eddy covariance measurements; HCB collected the CO_2 fugacity data; and JK, AE, and BS collected the surfactant data. The dual-tracer data were provided by RD and DH. HC collected the spar buoy measurements. YD prepared the first draft of the manuscript, and all co-authors contributed to and approved the final version.

Competing interests

The authors declare that they have no conflict of interest.

Disclaimer

Copernicus Publications remains neutral with regard to jurisdictional claims made in the text, published maps, institutional affiliations, or any other geographical representation in this paper. While Copernicus Publications makes every effort to include appropriate place names, the final responsibility lies with the authors. Views expressed in the text are those of the authors and do not necessarily reflect the views of the publisher

Acknowledgements

We thank the captains and crew of the *RV Elisabeth Mann Borgese*, T. Steffens (GEOMAR) for running the CO_2 flux system, and Matthis Björner and Michael Glockzin (IOW) for running/postprocessing the MESS data. We greatly appreciate F. Göhring (Deutscher Wetterdienst), Dr. M. Yang (Plymouth Marine Laboratory), Dr. J. Bidlot (European Centre for Medium-Range Weather Forecasts), Dr. A. Rutgersson (Uppsala University), Dr. J. Edson (Woods Hole Oceanographic Institution), and A. Körtzinger for helpful discussions. Data analysis and

https://doi.org/10.5194/egusphere-2025-6095
Preprint. Discussion started: 19 January 2026

visualization were completed using Python. ChatGPT was used in carefully polishing the manuscript' language to improve readability.

Financial support

In this study, Y. Dong has been supported by the Alexander von Humboldt Foundation. R. Dobashi acknowledges the support from Crown Prince Akihito Scholarship and the Uehiro Foundation on Ethics and Education. The ICOS station Östergarnsholm is funded by the Swedish Research Council and Uppsala University.

https://doi.org/10.5194/egusphere-2025-6095
Preprint. Discussion started: 19 January 2026

Reference

Bell, T. G., Landwehr, S., Miller, S. D., De Bruyn, W. J., Callaghan, A. H., Scanlon, B., et al.: Estimation of bubble-mediated air-sea gas exchange from concurrent DMS and CO_2 transfer velocities at intermediate-high wind speeds, Atmos. Chem. Phys., 17, 9019–9033, https://doi.org/10.5194/acp-17-9019-2017, 2017.

Bessonova, V., Tapoglou, E., Dorrell, R., Dethlefs, N., & York, K.: Global evaluation of wave data reanalysis: Comparison of the ERA5 dataset to buoy observations, Appl. Ocean Res., 157, 104490, https://doi.org/10.1016/j.apor.2025.104490, 2025.

Bittig, H. C., Jacobs, E., Neumann, T., & Rehder, G.: A regional pCO_2 climatology of the Baltic Sea from in situ pCO_2 observations and a model-based extrapolation approach, Earth Syst. Sci. Data, 16, 753–773, https://doi.org/10.5194/essd-16-753-2024, 2024.

Blomquist, B. W., Brumer, S. E., Fairall, C. W., Huebert, B. J., Zappa, C. J., Brooks, I. M., et al.: Wind speed and sea state dependencies of air-sea gas transfer: Results from the High Wind Speed Gas Exchange Study (HiWinGS), J. Geophys. Res. Oceans, 122, 8034–8062, https://doi.org/10.1002/2017JC013181, 2017.

Blomquist, B. W., Huebert, B. J., Fairall, C. W., Bariteau, L., Edson, J. B., Hare, J. E., & McGillis, W. R.: Advances in air-sea CO_2 flux measurement by eddy correlation, Bound.-Lay. Meteorol., 152, 245–276, https://doi.org/10.1007/s10546-014-9926-2, 2014.

Bock, E. J., Hara, T., Frew, N. M., & McGillis, W. R.: Relationship between air-sea gas transfer and short wind waves, J. Geophys. Res. Oceans, 104, 25821–25831, https://doi.org/10.1029/1999JC900200, 1999.

Brockmann, U. H., Huhnerfuss, H., Kattner, G., Broecker, H., & Hentzschel, G.: Artificial surface films in the sea area near Sylt 1, Limnol. Oceanogr., 27, 1050–1058, https://doi.org/10.4319/lo.1982.27.6.1050, 1982.

Brumer, S. E., Zappa, C. J., Blomquist, B. W., Fairall, C. W., Cifuentes-Lorenzen, A., Edson, J. B., et al.: Wave-related Reynolds number parameterizations of CO_2 and DMS transfer velocities, Geophys. Res. Lett., 44, 9865–9875, https://doi.org/10.1002/2017GL074979, 2017.

https://doi.org/10.5194/egusphere-2025-6095
Preprint. Discussion started: 19 January 2026

739 Brumer, S. E., Zappa, C. J., Brooks, I. M., Tamura, H., Brown, S. M., Blomquist, B. W., et al.:
740 Whitecap coverage dependence on wind and wave statistics as observed during SO GasEx and
741 HiWinGS, J. Phys. Oceanogr., 47, 2211–2235, https://doi.org/10.1175/JPO-D-17-0005.1, 2017.

742 Bullister, J. L., & Weiss, R. F.: Determination of CCl_3F and CCl_2F_2 in seawater and air, Deep-
743 Sea Res. Pt. A, 35, 839–853, https://doi.org/10.1016/0198-0149(88)90033-7, 1988.

744 Cole, J. J., & Caraco, N. F.: Atmospheric exchange of carbon dioxide in a low-wind oligotrophic
745 lake measured by the addition of SF6, Limnol. Oceanogr., 43, 647–656,
746 https://doi.org/10.4319/lo.1998.43.4.0647, 1998.

747 Cosović, B., & Vojvodić, V.: The application of ac polarography to the determination of surface-
748 active substances in seawater 1, Limnol. Oceanogr., 27, 361–369,
749 https://doi.org/10.4319/lo.1982.27.2.0361, 1982.

750 Cunliffe, M., & Wurl, O.: Guide to best practices to study the ocean's surface, Marine Biological
751 Association of the United Kingdom for SCOR, Plymouth, UK, http://plymsea.ac.uk/6523, 2014.

752 Deike, L.: Mass transfer at the ocean-atmosphere interface: The role of wave breaking, droplets,
753 and bubbles, Annu. Rev. Fluid Mech., 54, 191–224, https://doi.org/10.1146/annurev-fluid-
754 030121-014132, 2021.

755 Deike, L., & Melville, W. K.: Gas transfer by breaking waves, Geophys. Res. Lett., 45, 10482–
756 10492, https://doi.org/10.1029/2018GL078758, 2018.

757 Dobashi, R., & Ho, D. T.: Air-sea gas exchange in a seagrass ecosystem–results from a 3He/SF6
758 tracer release experiment, Biogeosciences, 20, 1075–1087, https://doi.org/10.5194/bg-20-1075-
759 2023, 2023.

760 Doney, S. C., Wolfe, W. H., McKee, D. C., & Fuhrman, J. G.: The science, engineering, and
761 validation of marine carbon dioxide removal and storage, Annu. Rev. Mar. Sci., 16, 1–27,
762 https://doi.org/10.1146/annurev-marine-040523-014702, 2024.

763 Dong, Y., Yang, M., Bakker, D. C. E., Kitidis, V., & Bell, T. G.: Uncertainties in eddy
764 covariance air-sea CO_2 flux measurements and implications for gas transfer velocity
765 parameterisations, Atmos. Chem. Phys., 21, 8089–8110, https://doi.org/10.5194/acp-21-8089-
766 2021, 2021.

https://doi.org/10.5194/egusphere-2025-6095
Preprint. Discussion started: 19 January 2026

Dong, Y., Jähne, B., Woolf, D. K., Krall, K. E., Yang, M., Czerski, H., et al.: The role of bubbles in air-sea gas exchange: A critical review, Authorea [preprint], https://doi.org/10.22541/essoar.175611263.31332921/v1, 2025.

Durrant, T. H., Greenslade, D. J. M., & Simmonds, I.: The effect of statistical wind corrections on global wave forecasts, Ocean Model., 70, 116–131, https://doi.org/10.1016/j.ocemod.2012.10.006, 2013.

Edson, J. B., Hinton, A. A., Prada, K. E., Hare, J. E., & Fairall, C. W.: Direct covariance flux estimates from mobile platforms at sea, J. Atmos. Ocean. Technol., 15, 547–562, https://doi.org/10.1175/1520-0426(1998)015<0547:DCFEFM>2.0.CO;2, 1998.

Edson, J. B., Jampana, V., Weller, R. A., Bigorre, S. P., Plueddemann, A. J., Fairall, C. W., et al.: On the exchange of momentum over the open ocean, J. Phys. Oceanogr., 43, 1589–1610, https://doi.org/10.1175/JPO-D-12-0173.1, 2013.

Fairall, C. W., Bariteau, L., Grachev, A. A., Hill, R. J., Wolfe, D. E., Brewer, W. A., et al.: Turbulent bulk transfer coefficients and ozone deposition velocity in the International Consortium for Atmospheric Research into Transport and Transformation, J. Geophys. Res. Atmos., 111, 1–19, https://doi.org/10.1029/2006JD007597, 2006.

Fairall, C. W., Yang, M., Brumer, S. E., Blomquist, B. W., Edson, J. B., Zappa, C. J., et al.: Air-sea trace gas fluxes: Direct and indirect measurements, Front. Mar. Sci., 9, 1–16, https://doi.org/10.3389/fmars.2022.826606, 2022.

Frew, N. M.: The role of organic films in air-sea gas exchange, in: The Sea Surface and Global Change, 121–172, https://doi.org/10.1017/CBO9780511525025.006, 1997.

Frew, N. M., Goldman, J. C., Dennett, M. R., & Johnson, A. S.: Impact of phytoplankton-generated surfactants on air-sea gas exchange, J. Geophys. Res. Oceans, 95, 3337–3352, https://doi.org/10.1029/JC095iC03p03337, 1990.

Frew, N. M., Bock, E. J., Schimpf, U., Hara, T., Haußecker, H., Edson, J. B., et al.: Air-sea gas transfer: Its dependence on wind stress, small-scale roughness, and surface films, J. Geophys. Res. Oceans, 109, 1–23, https://doi.org/10.1029/2003JC002131, 2004.

https://doi.org/10.5194/egusphere-2025-6095
Preprint. Discussion started: 19 January 2026

Friedlingstein, P., O'Sullivan, M., Jones, M. W., Andrew, R. M., Hauck, J., Landschützer, P., et al.: Global Carbon Budget 2024, Earth Syst. Sci. Data, 17, 965–1039, https://doi.org/10.5194/essd-17-965-2025, 2025.

Garbe, C. S., Rutgersson, A., Boutin, J., De Leeuw, G., Delille, B., Fairall, C. W., et al.: Transfer across the air-sea interface, in: Ocean-atmosphere interactions of gases and particles, 55–112, Springer, Berlin, Heidelberg, https://doi.org/10.1007/978-3-642-25643-1_2, 2014.

Gerke, L., Arck, Y., & Tanhua, T.: Temporal variability of ventilation in the Eurasian Arctic Ocean, J. Geophys. Res. Oceans, 129, e2023JC020608, https://doi.org/10.1029/2023JC020608, 2024.

Giudici, A., Jankowski, M. Z., Männikus, R., Najafzadeh, F., Suursaar, Ü., & Soomere, T.: A comparison of Baltic Sea wave properties simulated using two modelled wind data sets, Estuar. Coast. Shelf Sci., 290, 108401, https://doi.org/10.1016/j.ecss.2023.108401, 2023.

Goldman, J. C., Dennett, M. R., & Frew, N. M.: Surfactant effects on air-sea gas exchange under turbulent conditions, Deep-Sea Res. Pt. A, 35, 1953–1970, https://doi.org/10.1016/0198-0149(88)90119-7, 1988.

Gutiérrez-Loza, L., Nilsson, E., Wallin, M. B., Sahlée, E., & Rutgersson, A.: On physical mechanisms controlling air-sea CO_2 exchange, Biogeosciences, 19, 5645–5665, https://doi.org/10.5194/bg-19-5645-2022, 2022.

Hammer, K., Schneider, B., Kuliński, K., & Schulz-Bull, D. E.: Acid-base properties of Baltic Sea dissolved organic matter, J. Mar. Syst., 173, 114–121, https://doi.org/10.1016/j.jmarsys.2017.04.007, 2017.

Harvey, G. W., & Burzell, L. A.: A simple microlayer method for small samples 1, Limnol. Oceanogr., 17, 156–157, https://doi.org/10.4319/lo.1972.17.1.0156, 1972.

Ho, D. T., & Wanninkhof, R.: Air-sea gas exchange in the North Atlantic: $^3He/SF_6$ experiment during GasEx-98, Tellus B, 68, 30198, https://doi.org/10.3402/tellusb.v68.30198, 2016.

Ho, D. T., Schlosser, P., & Caplow, T.: Determination of longitudinal dispersion coefficient and net advection in the tidal Hudson River with a large-scale, high resolution SF_6 tracer release experiment, Environ. Sci. Technol., 36, 3234–3241, https://doi.org/10.1021/es015814, 2002.

https://doi.org/10.5194/egusphere-2025-6095
Preprint. Discussion started: 19 January 2026

Ho, D. T., Law, C. S., Smith, M. J., Schlosser, P., Harvey, M., & Hill, P.: Measurements of air-sea gas exchange at high wind speeds in the Southern Ocean: Implications for global parameterizations, Geophys. Res. Lett., 33, L16611, https://doi.org/10.1029/2006GL026817, 2006.

Ho, D. T., Bopp, L., Palter, J., Long, M. C., Boyd, P., Neukermans, G., & Bach, L.: Monitoring, reporting, and verification for ocean alkalinity enhancement, in: Guide to Best Practices in Ocean Alkalinity Enhancement Research, 2-oae2023, 1–12, https://doi.org/10.5194/sp-2023-2, 2023.

Jähne, B. J., Münnich, K. O. M., Bösinger, R., Dutzi, A., Huber, W., & Libner, P.: On the parameters influencing air-water gas exchange, J. Geophys. Res., 92, 1937–1949, https://doi.org/10.1029/JC092iC02p01937, 1987.

Klavins, M., & Purmalis, O.: Humic substances as surfactants, Environ. Chem. Lett., 8, 349–354, https://doi.org/10.1007/s10311-009-0232-z, 2010.

Kunz, J., & Jähne, B.: Investigating small-scale air–sea exchange processes via thermography, Front. Mech. Eng., 4, 4, https://doi.org/10.3389/fmech.2018.00004, 2018.

Kuss, J., Nagel, K., & Schneider, B.: Evidence from the Baltic Sea for an enhanced CO_2 air-sea transfer velocity, Tellus B, 56, 175, https://doi.org/10.3402/tellusb.v56i2.16407, 2004.

Landwehr, S., Miller, S. D., Smith, M. J., Bell, T. G., Saltzman, E. S., & Ward, B.: Using eddy covariance to measure the dependence of air-sea CO_2 exchange rate on friction velocity, Atmos. Chem. Phys., 18, 4297–4315, https://doi.org/10.5194/acp-18-4297-2018, 2018.

Landwehr, S., Thurnherr, I., Cassar, N., Gysel-Beer, M., & Schmale, J.: Using global reanalysis data to quantify and correct airflow distortion bias in shipborne wind speed measurements, Atmos. Meas. Tech., 13, 3487–3506, https://doi.org/10.5194/amt-13-3487-2020, 2020.

De Leeuw, G., Andreas, E. L., Anguelova, M. D., Fairall, C. W., Lewis, E. R., O'Dowd, C., et al.: Production flux of sea spray aerosol, Rev. Geophys., 49, 1–39, https://doi.org/10.1029/2010RG000349, 2011.

McGillis, W. R., Edson, J. B., Ware, J. D., Dacey, J. W. H., Hare, J. E., Fairall, C. W., & Wanninkhof, R.: Carbon dioxide flux techniques performed during GasEx-98, Mar. Chem., 75, 267–280, https://doi.org/10.1016/S0304-4203(01)00042-1, 2001.

https://doi.org/10.5194/egusphere-2025-6095
Preprint. Discussion started: 19 January 2026

McGillis, W. R., Edson, J. B., Zappa, C. J., Ware, J. D., McKenna, S. P., Terray, E. A., et al.: Air-sea CO_2 exchange in the equatorial Pacific, J. Geophys. Res. Oceans, 109, C08S90, https://doi.org/10.1029/2003JC002256, 2004.

McKenna, S. P., & McGillis, W. R.: The role of free-surface turbulence and surfactants in air–water gas transfer, Int. J. Heat Mass Transfer, 47, 539–553, https://doi.org/10.1016/j.ijheatmasstransfer.2003.06.001, 2004.

Mesarchaki, E., Kräuter, C., Krall, K. E., Bopp, M., Helleis, F., Williams, J., & Jähne, B.: Measuring air-sea gas-exchange velocities in a large-scale annular wind-wave tank, Ocean Sci., 11, 121–138, https://doi.org/10.5194/os-11-121-2015, 2015.

Miller, S. D., Marandino, C., & Saltzman, E. S.: Ship-based measurement of air-sea CO_2 exchange by eddy covariance, J. Geophys. Res. Atmos., 115, D02112, https://doi.org/10.1029/2009JD012193, 2010.

Moat, B., & Yelland, M.: Airflow distortion at instrument sites on the RRS James Clark Ross during the WAGES project, Natl. Oceanogr. Cent. Internal Doc., 12, http://nora.nerc.ac.uk/id/eprint/509304, 2015.

Moat, B. I., Yelland, M. J., & Cooper, E. B.: The airflow distortion at instruments sites on the RRS "James Cook", Natl. Oceanogr. Cent. Southampton Res. Consult. Rep., 11, 44 pp., http://eprints.soton.ac.uk/id/eprint/41147, 2006.

Mustaffa, N. I. H., Ribas-Ribas, M., Banko-Kubis, H. M., & Wurl, O.: Global reduction of in situ CO_2 transfer velocity by natural surfactants in the sea-surface microlayer, Proc. R. Soc. A, 476, 20190763, https://doi.org/10.1098/rspa.2019.0763, 2020.

Nightingale, P. D., Malin, G., Law, C. S., Watson, A. J., Liss, P. S., Liddicoat, M. I., et al.: In situ evaluation of air-sea gas exchange parameterizations using novel conservative and volatile tracers, Glob. Biogeochem. Cycles, 14, 373–387, https://doi.org/10.1029/1999GB900091, 2000.

O'Sullivan, N., Landwehr, S., & Ward, B.: Mapping flow distortion on oceanographic platforms using computational fluid dynamics, Ocean Sci., 9, 855–866, https://doi.org/10.5194/os-9-855-2013, 2013.

https://doi.org/10.5194/egusphere-2025-6095
Preprint. Discussion started: 19 January 2026

878 Ocampo-Torres, F. J., & Donelan, M. A.: On the influence of fetch and the wave field on the
879 CO_2 transfer process: Laboratory measurements, in: Air–Water Gas Transfer, B. Jähne &
880 E. C. Monahan (Eds.), AEON Verlag & Studio, Hanau, 543–552, 1995.

881 Parard, G., Charantonis, A. A., & Rutgersson, A.: Using satellite data to estimate partial pressure
882 of CO_2 in the Baltic Sea, J. Geophys. Res. Biogeosci., 121, 1002–1015,
883 https://doi.org/10.1002/2015JG003064, 2016.

884 Pereira, R., Schneider-Zapp, K., & Upstill-Goddard, R. C.: Surfactant control of gas transfer
885 velocity along an offshore coastal transect: Results from a laboratory gas exchange tank,
886 Biogeosciences, 13, 3981–3989, https://doi.org/10.5194/bg-13-3981-2016, 2016.

887 Pereira, R., Ashton, I., Sabbaghzadeh, B., Shutler, J. D., & Upstill-Goddard, R. C.: Reduced air-
888 sea CO_2 exchange in the Atlantic Ocean due to biological surfactants, Nat. Geosci., 11, 492–496,
889 https://doi.org/10.1038/s41561-018-0136-2, 2018.

890 Pitarch, J., Volpe, G., Colella, S., Krasemann, H., & Santoleri, R.: Remote sensing of chlorophyll
891 in the Baltic Sea at basin scale from 1997 to 2012 using merged multi-sensor data, Ocean Sci.,
892 12, 379–389, https://doi.org/10.5194/os-12-379-2016, 2016.

893 Prytherch, J., & Yelland, M. J.: Wind, convection and fetch dependence of gas transfer velocity
894 in an Arctic sea-ice lead determined from eddy covariance CO_2 flux measurements, Glob.
895 Biogeochem. Cycles, 35, e2020GB006633, https://doi.org/10.1029/2020GB006633, 2021.

896 Resplandy, L., Hogikyan, A., Müller, J. D., Najjar, R. G., Bange, H. W., Bianchi, D., et al.: A
897 synthesis of global coastal ocean greenhouse gas fluxes, Glob. Biogeochem. Cycles, 38, 1–38,
898 https://doi.org/10.1029/2023GB007803, 2024.

899 Ribas-Ribas, M., Helleis, F., Rahlff, J., & Wurl, O.: Air-sea CO_2 exchange in a large annular
900 wind-wave tank and the effects of surfactants, Front. Mar. Sci., 5, 457,
901 https://doi.org/10.3389/fmars.2018.00457, 2018.

902 Rutgersson, A., & Smedman, A.: Enhanced air-sea CO_2 transfer due to water-side convection, J.
903 Mar. Syst., 80, 125–134, https://doi.org/10.1016/j.jmarsys.2009.11.004, 2010.

904 Rutgersson, A., Pettersson, H., Nilsson, E., Bergström, H., Wallin, M. B., Nilsson, E. D., et al.:
905 Using land-based stations for air-sea interaction studies, Tellus A, 72, 1–23,
906 https://doi.org/10.1080/16000870.2019.1697601, 2020.

https://doi.org/10.5194/egusphere-2025-6095
Preprint. Discussion started: 19 January 2026

907 Sabbaghzadeh, B., Upstill-Goddard, R. C., Beale, R., Pereira, R., & Nightingale, P. D.: The
908 Atlantic Ocean surface microlayer from 50°N to 50°S is ubiquitously enriched in surfactants at
909 wind speeds up to 13 m s^{-1}, Geophys. Res. Lett., 44, 2852–2858,
910 https://doi.org/10.1002/2017GL072988, 2017.

911 Sabbaghzadeh, B., Arévalo-Martínez, D. L., Glockzin, M., Otto, S., & Rehder, G.: Meridional
912 and cross-shelf variability of N_2O and CH_4 in the eastern-south Atlantic, J. Geophys. Res.
913 Oceans, 126, e2020JC016878, https://doi.org/10.1029/2020JC016878, 2021.

914 Salter, M. E., Upstill-Goddard, R. C., Nightingale, P. D., Archer, S. D., Blomquist, B., Ho, D. T.,
915 et al.: Impact of an artificial surfactant release on air-sea gas fluxes during Deep Ocean Gas
916 Exchange Experiment II, J. Geophys. Res. Oceans, 116, C11007,
917 https://doi.org/10.1029/2011JC007023, 2011.

918 Schmidt, R., & Schneider, B.: The effect of surface films on the air-sea gas exchange in the
919 Baltic Sea, Mar. Chem., 126, 56–62, https://doi.org/10.1016/j.marchem.2011.03.007, 2011.

920 Sültenfuß, J., Roether, W., & Rhein, M.: The Bremen mass spectrometric facility for the
921 measurement of helium isotopes, neon, and tritium in water, Isot. Environ. Health Stud., 45, 83–
922 95, https://doi.org/10.1080/10256010902871929, 2009.

923 Upstill-Goddard, R. C.: Air-sea gas exchange in the coastal zone, Estuar. Coast. Shelf Sci., 70,
924 388–404, https://doi.org/10.1016/j.ecss.2006.05.043, 2006.

925 Vickers, D., & Mahrt, L.: Fetch limited drag coefficients, Bound.-Lay. Meteorol., 85, 53–79,
926 https://doi.org/10.1023/A:1000472623187, 1997.

927 Wanninkhof, R.: Relationship between wind speed and gas exchange over the ocean revisited,
928 Limnol. Oceanogr. Methods, 12, 351–362, https://doi.org/10.4319/lom.2014.12.351, 2014.

929 Wanninkhof, R., Asher, W. E., Ho, D. T., Sweeney, C., & McGillis, W. R.: Advances in
930 quantifying air-sea gas exchange and environmental forcing, Annu. Rev. Mar. Sci., 1, 213–244,
931 https://doi.org/10.1146/annurev.marine.010908.163742, 2009.

932 Weiss, R. F.: Carbon dioxide in water and seawater: the solubility of a non-ideal gas, Mar.
933 Chem., 2, 203–215, https://doi.org/10.1016/0304-4203(74)90015-2, 1974.

https://doi.org/10.5194/egusphere-2025-6095
Preprint. Discussion started: 19 January 2026

Woolf, D. K., Land, P. E., Shutler, J. D., Goddijn-Murphy, L. M., & Donlon, C. J.: On the calculation of air-sea fluxes of CO_2 in the presence of temperature and salinity gradients, J. Geophys. Res. Oceans, 121, 1229–1248, https://doi.org/10.1002/2015JC011427, 2016.

Woolf, D. K.: Bubbles and the air-sea transfer velocity of gases, Atmos.-Ocean, 31, 517–540, https://doi.org/10.1080/07055900.1993.9649484, 1993.

Woolf, D. K.: Parametrization of gas transfer velocities and sea-state-dependent wave breaking, Tellus B, 57, 87, https://doi.org/10.3402/tellusb.v57i2.16783, 2005.

Woolf, D. K.: Bubbles and their role in gas exchange, in: The Sea Surface and Global Change, 173–206, Cambridge University Press, https://doi.org/10.1017/CBO9780511525025.007, 1997.

Wurl, O., Wurl, E., Miller, L., Johnson, K., & Vagle, S.: Formation and global distribution of sea-surface microlayers, Biogeosciences, 8, 121–135, https://doi.org/10.5194/bg-8-121-2011, 2011.

Yang, M., Smyth, T. J., Kitidis, V., Brown, I. J., Wohl, C., Yelland, M. J., & Bell, T. G.: Natural variability in air-sea gas transfer efficiency of CO_2, Sci. Rep., 11, 1–9, https://doi.org/10.1038/s41598-021-92947-w, 2021.

Yang, M., Bell, T. G., Bidlot, J. R., Blomquist, B. W., Butterworth, B. J., Dong, Y., et al.: Global synthesis of air-Sea CO_2 transfer velocity estimates from ship-based eddy covariance measurements, Front. Mar. Sci., 9, 1–15, https://doi.org/10.3389/fmars.2022.826421, 2022.

Yang, M., Moffat, D., Dong, Y., & Bidlot, J.-R.: Deciphering the variability in air-sea gas transfer due to sea state and wind history, PNAS Nexus, pgae389, https://doi.org/10.1093/pnasnexus/pgae389, 2024.

Zhao, D., Toba, Y., Suzuki, Y., & Komori, S.: Effect of wind waves on air-sea gas exchange: Proposal of an overall CO_2 transfer velocity formula as a function of breaking-wave parameter, Tellus B, 55, 478–487, https://doi.org/10.3402/tellusb.v55i2.16747, 2003.